

Advanced Gradient Heating Facility (AGHF)

*08/11/2011*

## Coupled Growth in Hypermonotectics

Principal Investigator:

Dr. J. Barry Andrews  
University of Alabama at Birmingham  
Birmingham, Alabama

# Coupled Growth in Hypermonotectics

J. Barry Andrews\* and Sam R. Coriell\*\*

\*University of Alabama at Birmingham

Birmingham, AL 35294

\*\*National Institute of Standards and Technology

Gaithersburg, MD 20899

## OBJECTIVE

The primary objective of this project is to obtain a better understanding of solidification processes in immiscible alloy systems. While many alloys in these systems show great potential for use in engineering applications (in particular for superconductors, bearings, catalysts, electrical contacts, and magnetic materials) control of the solidification process is difficult due to gravitationally imposed flows and sedimentation. This project makes use of the low-g environment available during low-Earth orbit to obtain samples solidified without the deleterious influence of gravity. The experimental results are compared to those obtained from modeling the solidification process and are used to help enhance the models developed. Success in this effort will eventually lead to an improved knowledge of ways in which to control microstructures developed in these intriguing alloys.

## BACKGROUND

Two-liquid immiscibility is usually associated with a monotectic alloy system, an example of which is represented by the phase diagram in Figure 1. One of the most prominent features of this phase diagram is the miscibility gap in which two separate liquids co-exist over a temperature and composition range. It is also apparent that a transformation can occur in this system which involves the decomposition of one liquid phase to form a solid and another liquid phase (i.e. the monotectic reaction  $L_1 \rightarrow S_1 + L_2$ ).

The monotectic reaction is similar to another type of reaction, called the eutectic reaction, which occurs in many alloy systems ( $L \rightarrow S_1 + S_2$ ). As a result, some of the theoretical work carried out on eutectics can provide a starting point for the development of a model for monotectics. However, the fact that one of the product phases in a monotectic is a liquid can lead to substantially different behavior than that observed in eutectic systems where both product phases are solids.

One of the useful features of eutectic alloy systems is that by directionally solidifying the alloys under the proper conditions, a structure can be obtained which consists of aligned fibers of one phase in a matrix of the other. This fibrous composite structure forms as a result of the unmixing of the liquid phase to form the two product phases. In this reaction the solute rejected during the formation of one of the solid phases is consumed in the formation of the other solid phase. This "coupled growth" process has also been observed in some immiscible alloy systems for alloys of monotectic composition.

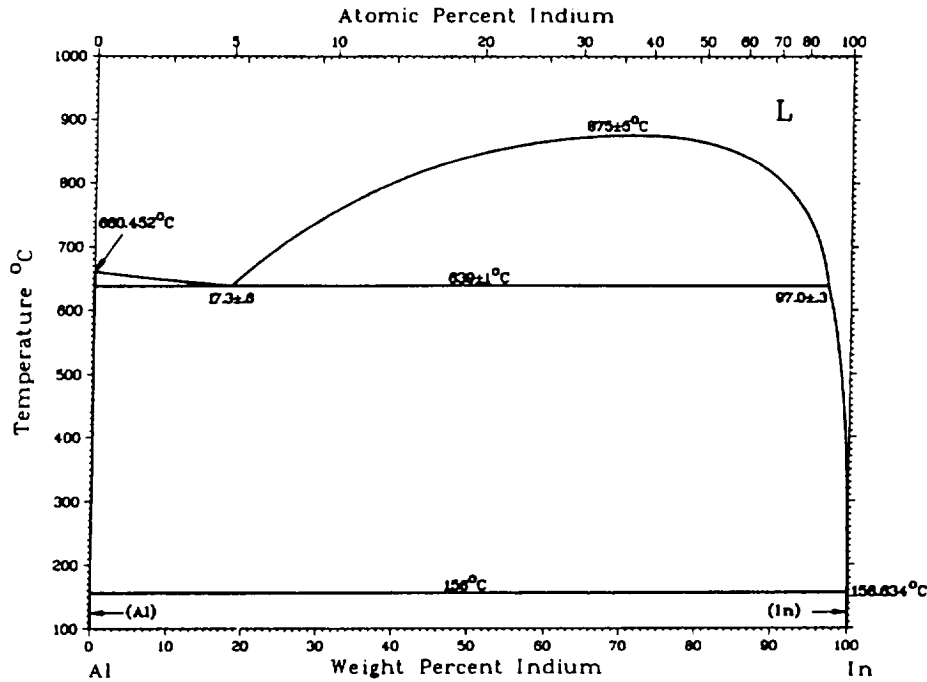


Figure 1. Phase diagram for the aluminum-indium alloy system

It is well known that in eutectic alloy systems, alloys which are off of eutectic composition can also be directionally solidified to produce fibrous microstructures. In fact, the use of off-eutectic compositions provides a means of controlling the volume fraction of the fibrous phase. However, there has been some controversy whether off-monotectic alloys, especially those with solute contents higher than the monotectic (i.e. hypermonotectic alloys) can be directionally solidified under conditions which would lead to a stable coupled growth process and the development of a fibrous microstructure.

As seen in an off-eutectic alloy, steady state coupled growth in an off-monotectic alloy should involve two diffusion fields. One of these fields would be associated with the “unmixing” process, which is part of coupled growth. This diffusion field should only extend into the liquid a short distance, approximately one half the interfiber spacing. The other diffusion field would arise due to the alloy being off of monotectic composition. The composition of the liquid far removed from the solidification front would be equal to the alloy composition, while the composition at the front would be held at the monotectic composition. This composition variation, which would occur primarily close to the solidification front, is called the solute boundary layer.

The presence of a solute boundary layer in the liquid in advance of the solidification front gives rise to the possibility of interfacial instability. The composition variation with position in the liquid results in a variation in the temperature at which the miscibility gap would be entered. Just adjacent to the interface, a temperature as low as the monotectic temperature can be tolerated without entering the miscibility gap. However, as the composition increases with distance from

the interface the temperature at which the miscibility gap would be entered increases as well. If the thermal gradient in the sample is insufficient to keep the local temperature above the local miscibility gap temperature, the second phase immiscible liquid can form in advance of the solidification front and disrupt the coupled growth process. The conditions which must be met in order to avoid this instability are given by the relationship

$$\frac{G_L}{V} > \frac{m_L (C_o - C_m)}{D_L}$$

where

- $G_L$  = temperature gradient in the liquid
- $V$  = solidification front velocity
- $m_L$  = slope of the ( $L_1 + L_2$ ) two-phase boundary
- $C_o$  = alloy composition
- $C_M$  = monotectic composition
- $D_L$  = diffusivity of solute in the liquid

If the above conditions are met it should be possible to produce an aligned fibrous composite microstructure even in a hypermonotectic alloy. It is important to note that since the formation of the  $L_2$  phase in advance of the solidification front can be suppressed, difficulties due to sedimentation of the  $L_2$  phase during directional solidification can be avoided. However, there are other gravity driven phenomena that make ground based experimentation difficult.

While the solute depleted boundary layer in advance of a solidification front should make it possible to achieve steady state coupled growth by using the proper growth conditions, this boundary layer may give rise to undesirable fluid flow in the sample. In almost every known immiscible alloy system the solute has a higher density than the solvent. This implies that for vertical solidification, the solute depleted boundary layer in advance of the solidification front will have a lower density than the liquid above it. This density variation is expected to result in convective flows which can lead to difficulties during solidification. In most cases the resulting convective flow can cause compositional variations that are sufficient to prevent coupled growth over a substantial portion of the sample.

In order to obtain steady state coupled growth conditions in immiscible alloys both interfacial stability and convective stability will be required. It should be possible to obtain interfacial stability by directionally solidifying alloys using a high thermal gradient to growth rate ratio. This requirement can best be met by using a furnace that can produce a high thermal gradient in the sample during solidification. Convective stability presents more of a problem. Analysis implies that the only way to reduce convective flows to the level required for this study is by carrying out directional solidification under microgravity conditions.

## DATA ACQUISITION AND ANALYSIS

The Coupled Growth in Hypermonotectics project involves the directional solidification of a range of alloy compositions over a range of growth rates. For the Life and Microgravity Spacelab (LMS) mission, three alloy compositions in the aluminum-indium immiscible system

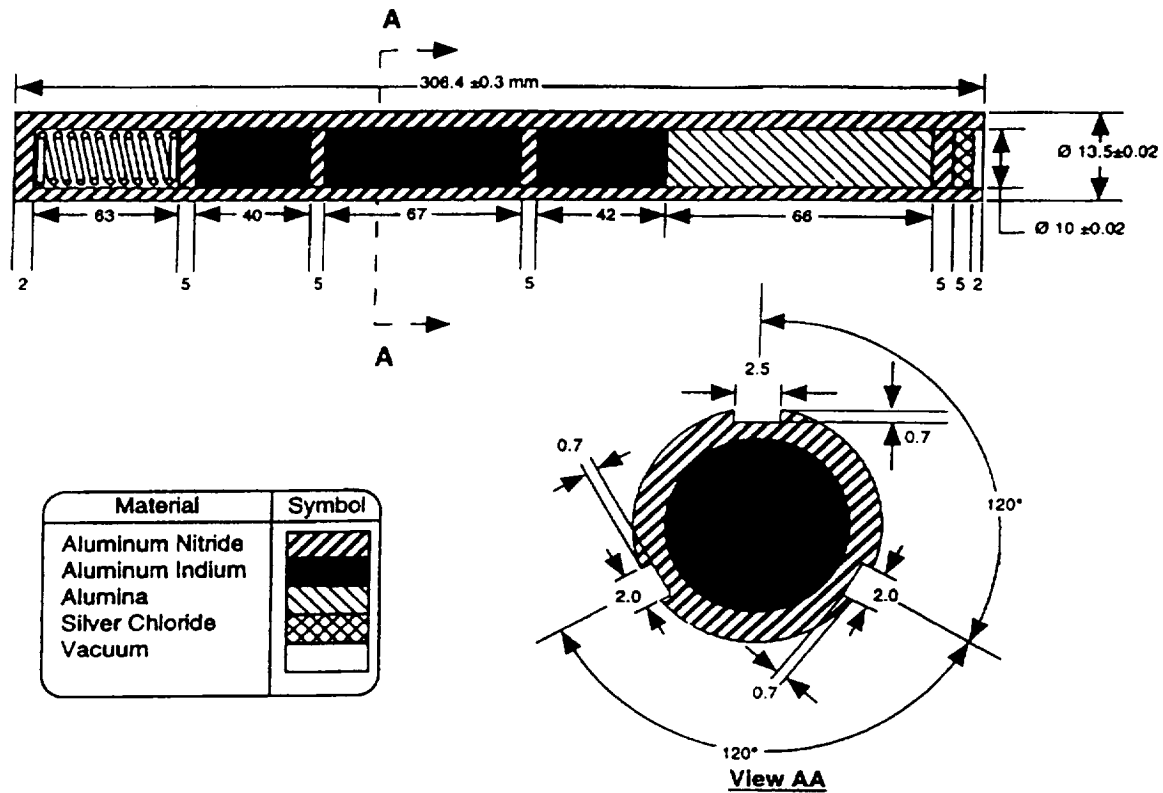


Figure 2. Schematic of the ampoule assembly utilized to process aluminum-indium immiscible alloys during the LMS mission.

were directionally solidified. The Advanced Gradient Heating Facility (AGHF) was used to directionally solidify these samples and all samples were solidified at the same rate of  $1.0 \mu\text{m/s}$ . The samples were sealed under vacuum in aluminum nitride ampoules which contained several sample segments, pistons and a spring in order to maintain the desired growth conditions during processing (See Figure 2). Thermocouples were embedded into the wall of the ampoule and were used to monitor temperatures and determine thermal gradients and growth rates. Alloys were produced from five-nines purity components and were vacuum induction melted.

A great deal of effort was used in the preparation of the alloy and ampoule assemblies in order to avoid the presence of any free surfaces or voids in the samples during processing. Free surfaces were undesirable because the surface tension driven flow at those surfaces could result in undesirable mixing within the sample. In order to avoid free surfaces generated due to contraction of the sample prior to and during solidification, a piston and high temperature carbon spring were utilized. In an attempt to reduce any residual gasses, which could have led to bubble formation, the alloys were vacuum induction melted. In addition, the ampoule components were all vacuum degassed at  $1250^\circ\text{C}$  for more than 6 hours. Samples were loaded and sealed under a vacuum of at least  $1 \times 10^{-4}$  Torr.

During processing, data was collected on furnace position, acceleration (3 axes), furnace translation rate, sample thermocouple outputs, and hot and cold zone temperatures.

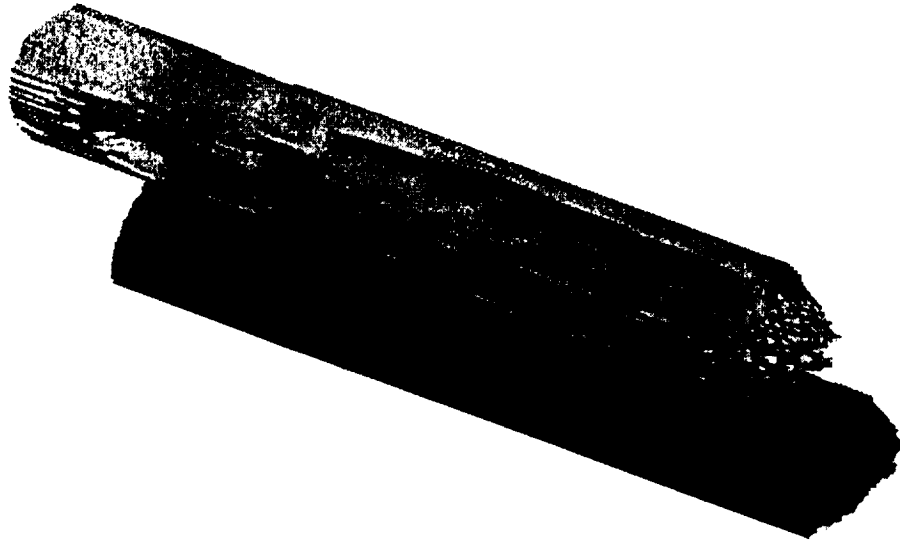


Figure 3. Computed tomography image obtained for the 18.5wt% In sample, FM 1.

Metallographic and compositional information is also to be obtained on these samples. The directionally solidified samples will be longitudinally sectioned and one of the sample halves mounted for metallographic analysis. The other half of the sample will be transversely sectioned and these sections used for compositional analysis (using precision density measurements) and then metallographic analysis. Analysis of the transverse sections will permit determination of interfiber spacings and the volume fractions of the phases along the length of the sample.

## RESULTS AND DISCUSSION

Several difficulties were encountered during processing of the CGH samples aboard LMS. The first difficulty concerned a thermal gradient in the flight furnace that was substantially lower than that obtained using the engineering model of the furnace. This reduced thermal gradient is expected to have a detrimental influence on the ability to maintain a stable solidification front, especially for the highest composition alloy. Another difficulty involved the loss of data telemetry from the AGHF during processing of the 18.5% In alloy. Several attempts were made to reestablish the data link without success. Unfortunately, there was no data recording capability within the AGHF facility so all data on furnace position and sample temperatures were lost for this sample.

Radiographic analysis and computed tomography of the samples while still in their ampoules revealed the presence of several significant sized voids in in two of the flight samples (See Figures 3, 4 and 5). These unexpected voids give rise to several difficulties. First, the voids provide free surfaces, which, with the high thermal gradients in this experiment can allow surface tension induced flow and undesirable mixing in the sample. However, perhaps an even worse problem is the inconsistency in growth conditions that will exist along the sample. The voids will obviously change the local cross sectional area of the sample and result in local variations in both thermal gradient and growth rate. These variations in local conditions will make analysis of the results much more difficult.

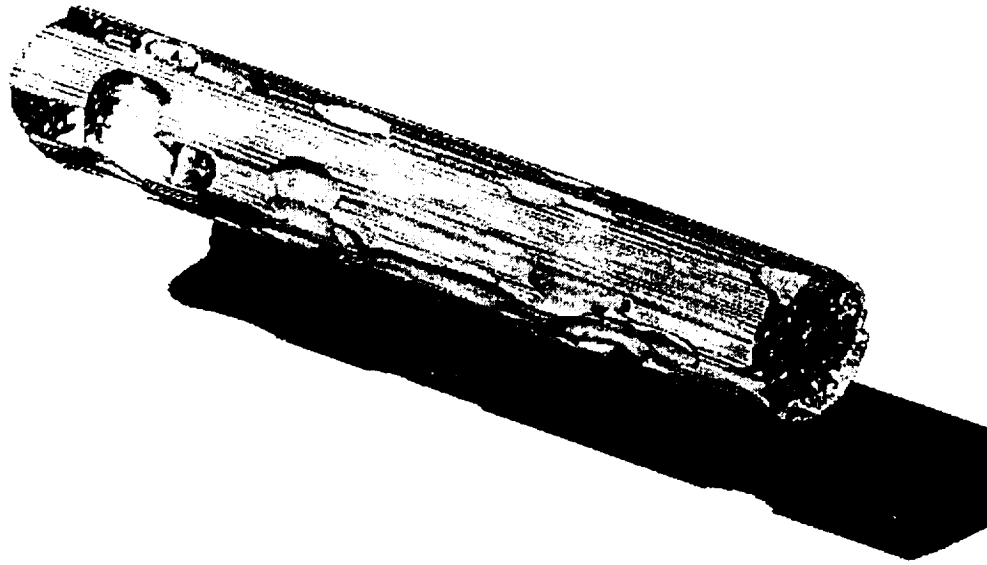


Figure 4. Computed tomography image of the 19.7wt% In, FM 2 sample.



One of the first questions which must be answered in this study concerns the source of these voids. This information is especially important since additional flight experiments are anticipated in this study. As a result, the primary focus of this project to date has been to determine the source of these unexpected voids.

There are several factors that could have led to the development of voids in these samples. For example, if the high temperature spring failed or if one of the pistons stuck, the ampoule would not be able to compensate for the thermal contraction in the melt or for the solidification shrinkage. This type of failure could result in the formation of voids. In several of the early experiments carried out during development of the ampoule assembly the aluminum-indium alloy leaked past the uppermost piston into the area containing the spring. At these elevated temperatures (1110° C) the carbon spring and aluminum react to form aluminum carbide, thus destroying the spring. After initial testing of the ampoule assembly, more stringent specifications were placed on the tolerances and surface finish for the ampoule bore and pistons. Further testing indicated this problem had been solved. However, it is apparent from post flight x-ray analysis of the ampoule assemblies that leakage into the spring area occurred in two of the flight ampoules and one of the ground based ampoules. Once this leakage occurred it is assumed the spring would have become ineffective.

Another factor that could lead to the development of voids in the samples is leakage of gas past the silver chloride seal at the bottom of the ampoule. Gas that entered the ampoule could result in bubble formation in the melt if the gas pressure within the bubble could not be overcome by the spring assembly. Each ampoule was helium leak tested after assembly in order to avoid this possibility. However, it is conceivable that changes in the integrity of the seal occurred during subsequent handling or during heating for processing.

Another possibility for gas bubble formation involves gas release from within the ampoule either due to decomposition of a component at temperature or due to a reaction. A reaction between the aluminum or indium and the aluminum nitride ampoule is not anticipated. In addition, reactions between the ampoule and carbon spring were not observed during testing. The vapor pressures of aluminum and indium are both rather low at the temperatures utilized and should be easily overcome by the spring pressure. However, it is still possible that some reaction is taking place that was overlooked.

Since this experiment is to fly on future missions, it was felt that identification of the source of the voids in these samples was a critical factor. Much insight could be gained by determining whether the voids contained a gas, and if so, the composition of that gas. As a result most of our recent efforts have focused on identifying the contents of the voids. The first thought was to open the ampoules in a vacuum chamber and to monitor the species released using a mass spectrometer. However, a survey of equipment at the University of Alabama at Birmingham and at Marshall Space Flight Center revealed that an appropriately sized chamber was not available and that mechanical manipulation within the chamber in order to open the ampoule was very limited. Further discussions led us to Dr. Witold Palosz at the Marshall Space Flight Center who has been using a specifically designed apparatus to determine residual gas content in fused silica ampoules used in semiconductor processing. Dr. Palosz's approach has been to break open an ampoule in a small vacuum chamber and determine the gas content by slowly lowering the

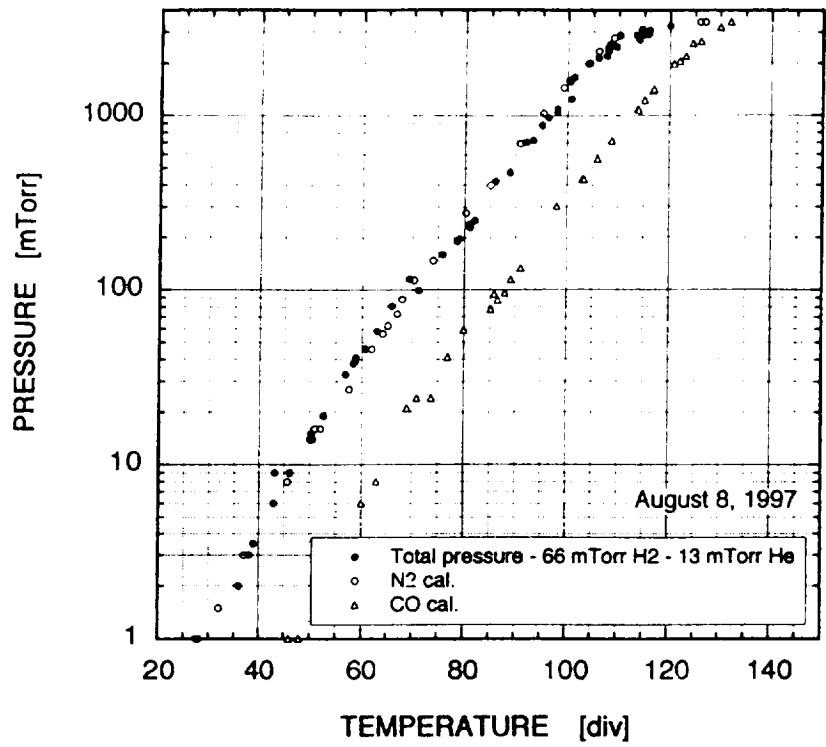


Figure 6. Pressure vs. temperature variations during a typical residual gas analysis. The open circles represent a nitrogen calibration curve while the open triangles represent a carbon monoxide calibration curve. The temperature scale covers a range of roughly 20K to 120K.

shown in Figure 6. This figure also contains calibration curves for nitrogen (open circles) and carbon monoxide (open triangles) which are the most difficult gases to distinguish by this technique.

The first sample tested in the system, sample FM1, exhibited behavior which was later found to be nontypical. After evacuating the system for one hour the sample was found to be out-gassing at a rate of 400mTorr/hr. After 20 hours total pumping time the out-gassing rate had dropped to 150m Torr/hr. The outgassing rate then dropped to 40mTorr/hr after a total of 46 hours and to 13 mTorr/hr after 66 hours. When the ampoule was opened only 0.06cm<sup>3</sup> of gas (at standard temperature and pressure) was released. These results indicate that a leak may have been present in this ampoule. All of the sealed ampoules were helium leak tested before being incorporated into the cartridge assemblies for processing. However, it is possible that the seal failed either during handling or during processing. Retesting of all of the ampoule seals is currently planned in order to determine if seal leakage was a contributing factor to void formation in some cases. Another possibility is that a hairline crack developed in the ampoule when the groove was cut to serve as a fracture site. Most of the other ampoule assemblies did not exhibit outgassing to this extent. In addition, as shown in Table 1, the volume of gas released when the other flight ampoules were opened was much more significant, giving volumes of 1.7 and 0.92 cm<sup>3</sup> at STP. Compositional analysis of the gas obtained from the flight ampoules revealed that a significant amount of nitrogen was present in all cases. While preliminary, indications are that carbon monoxide was also present in two of the ampoules. It is tempting to speculate on the source of this carbon monoxide, especially since this gas was found in the two ampoules in which the alloy leaked past the piston and came in contact with the carbon spring. However, additional calibration runs are necessary to verify the presence of carbon monoxide. These calibration runs are the next order of business.

The nitrogen found in these flight ampoules may have come from several sources. Of course, one possibility is from air which was either trapped in, or leaked into, the ampoule. Since the ampoules were sealed in a vacuum after an elevated temperature bakeout there should have been very little air initially present in the ampoules. Another possibility is due to breakdown of the aluminum nitride ampoule material at the elevated temperatures used during processing. While there is very little information available pertaining to this possibility, tests are currently being carried out to collect gases released by aluminum nitride during extended duration elevated temperature exposure.

Two ground based control samples were also processed as a part of this investigation. One of these samples, GM1, contained a rather large void in the cold load segment of the ampoule. Unfortunately, this ampoule was apparently cracked when the groove was cut to facilitate opening and a gas analysis could not be obtained. The remaining ground based ampoule, GM2, exhibited almost ideal behavior. The sample was essentially void free and no leakage occurred past the piston into the spring assembly. Analysis of the residual gas present in this ampoule revealed 0.34 cm<sup>3</sup> of almost pure hydrogen (at standard temperature and pressure) was present. Obviously this result is quite different than that observed in the other ampoules. We currently have no explanation for the source of this gas.

**Table 1: Preliminary Results from Residual Gas Analysis**

SAMPLE NUMBER	COMPOSITION (wt % In)	PRELIMINARY GAS COMPOSITION	GAS VOLUME AT STP(cm <sup>3</sup> )	COMMENTS
FM1	18.5	Nitrogen + some CO <sub>2</sub>	0.06	May have leaked
FM2	19.7	Nitrogen	1.73	
FM3	17.3	Mostly nitrogen some CO & H <sub>2</sub>	0.92	
GM1	18.5			Ampoule cracked
GM2	19.7	Almost all hydrogen	0.34	Essentially void free

## SUMMARY AND FUTURE PLANS

To summarize our findings to date, three immiscible aluminum indium samples were directionally solidified during the LMS mission. Two of these samples contained voids that were sufficient in size to modify the solidification parameters locally during processing. In addition, the aluminum-indium alloy leaked past the uppermost piston in two of the flight ampoules and one of the ground based ampoules and destroyed the carbon spring. Most work to date has concentrated on identifying the gas present in the voids in order to help determine their source.

Residual gas analysis revealed that the voids contained primarily nitrogen with some ampoules also containing smaller amounts of a gas, which, at this stage is thought to be carbon monoxide. Additional testing must be carried out to verify this finding. Analysis of one of the ground based ampoules revealed a residual gas composed almost entirely of hydrogen. This ground-based sample was essentially void free.

Much remains to be done in the analysis of these samples. Part of this work involves a continuation of the investigation of void formation. This will include collection and testing of any gases released during extended duration high temperature exposure of an ampoule. The seals for each ampoule will also be helium leak tested. Additional testing will be carried out to determine if the ampoules all met surface finish and tolerance specifications as well.

In addition to the work described above, an extensive amount of metallographic analysis remains to be done on these samples. This work will involve determination of the interfiber spacings and volume fractions of phases as a function of position along the samples. The findings from the metallographic analysis will be used to first determine if interface stability and coupled growth were obtained. The specific microstructural details will then be used to test the monotectic solidification model developed as part of this investigation.

**Bibliographic Citations of Articles/Presentations Resulting from the  
Flight for the Project:  
Coupled Growth in Hypermonotectics**

"Coupled Growth in Immiscible Alloys," J. B. Andrews, L. Hayes, Y. Arikawa, S. O'Dell, and A. Cheney, Space Processing of Materials, Proceedings SPIE - The International Society for Optical Engineering, ed. N. Ramachandran, Vol. 2809, pp. 12-22, 1996.

"Microgravity Processing of Immiscible Aluminum-Indium Alloys," J. B. Andrews, L. J. Hayes, Y. Arikawa, S. R. Coriell, accepted for publication in Advances in Space Research, 1997.

"Analysis of Monotectic Growth: Infinite Diffusion in the L<sub>1</sub> Phase," S. R. Coriell, W. F.

---

Mitchell, B. Murray, J. B. Andrews, Y. Arikawa, Journal of Crystal Growth, 1997.

"Directional Solidification of Immiscible Aluminum-Indium Alloys under Microgravity Conditions," J. B. Andrews, L. J. Hayes, Y. Arikawa and S. R. Coriell, Proceedings - Spacebound '97 and Proceedings of the 9<sup>th</sup> International Symposium on Experimental Methods for Microgravity Materials Science, accepted for publication in both.

"The Influence of Convection in Directionally Solidified Hypermonotectic Alloys," L. J. Hayes and J. B. Andrews, Proceedings - Spacebound '97 and Proceedings of the 9<sup>th</sup> International Symposium on Experimental Methods for Microgravity Materials Science, accepted for publication in both.

"Numerical Simulation of a Monotectic Solidification Front with Marangoni Flow," Y. Arikawa, J. B. Andrews, S. R. Coriell, W. F. Mitchell, B. Murray, Proceedings - Spacebound '97 and Proceedings of the 9<sup>th</sup> International Symposium on Experimental Methods for Microgravity Materials Science, accepted for publication in both.

---

# **Coupled Growth in Hypermonotectics**

**J. Barry Andrews\* and Sam R. Coriell\*\***

**\*University of Alabama at Birmingham**

**Birmingham, AL 35294**

**\*\*National Institute of Standards and Technology**

**Gaithersburg, ME 20899**

## **NON-TECHNICAL SUMMARY**

Well over 1000 alloy systems exhibit immiscible behavior in the liquid state, where, like oil and water, two liquids form that do not mix. Many of these alloy systems show promise for use in engineering applications such as superconductors, high performance permanent magnets, electrical contact materials and catalysts. However, controlling the solidification process in order to produce desirable structures in these alloys is very difficult. An improved understanding of solidification processes is needed, but study of the solidification process on Earth is hindered by the inherent flows which occur in these systems and by the possibility of the heavier of the two liquid phases sinking to the bottom of the container during processing.

The objective of this investigation is to gain an improved understanding of solidification processes in immiscible alloy systems. A portion of the study involves the development of experimental techniques which will permit solidification of immiscible alloys to produce aligned microstructures. A parallel effort is underway to develop a model for the solidification process in these alloy systems. This analysis avoids many of the simplifying assumptions often utilized in similar analyses. Results from experimentation will be compared to those predicted from the model and utilized to improve the model. In order to permit solidification under the conditions necessary to form fibrous structures in these immiscible alloys, experimentation must be carried out under low-gravity conditions.

This experiment used the Advanced Gradient Heating Facility (AGHF) and low-gravity conditions to help remove the complications of sedimentation and buoyancy driven convective flow during directional solidification of immiscible alloys. Alloys in the aluminum indium system were solidified using specialized aluminum nitride ampoules in order to control several undesirable effects that are sometimes observed during low gravity processing. Three alloy compositions were processed in order to permit comparison with the model over a composition range. Two ground based control samples were processed under conditions identical to those of two of the flight samples in order to allow a direct comparison of the results.

Upon analysis several voids were found in two of the flight ampoules. The presence of these voids will present problems in the analysis of the samples since the voids can influence the solidification conditions locally. Most work to date has focused on identifying the gas present in these voids in an attempt to identify their source. Preliminary data has been collected and several experiments are underway in this area. The next step in the project will involve a detailed structural analysis of the samples.



Advanced Gradient Heating Facility (AGHF)

## Directional Solidification of Refined Al - 4 wt.% Cu Alloys

Principal Investigator:

Dr. Denis Camel  
DEM/SES  
Grenoble, France

# LMS-AGHF-ESA2b EXPERIMENT DIRECTIONAL SOLIDIFICATION OF REFINED Al-4wt.%Cu ALLOYS

M.D. DUPOUY, D. CAMEL, F. BOTALLA, J. ABADIE and J.J. FAVIER

Commissariat à l'Énergie Atomique - CEREM - Département d'Étude des Matériaux  
17 Rue des Martyrs, 38054 Grenoble Cédex 9, France

## (1) OBJECTIVES

In the case of directional solidification of inoculated alloys under diffusive transport conditions, the transition from columnar to equiaxed grain structure is predicted to occur continuously through intermediate mixed structures, as a function of the nuclei density  $N_0$ , temperature gradient  $G$  and solidification rate  $R$  [1]. The Hunt's model could not be verified experimentally [2, 3] because, in practice, gravity driven convection affects these three parameters. For this reason, more recent models [4, 5] try to include convective effects. However, in order to assess the models, experiments able to separate convection from the other mechanisms involved are still needed. The purpose of the LMS-AGHF-ESA2b experiment was to examine the columnar to equiaxed transition (CET) in a refined Al-4wt.%Cu alloy under conditions in which convection is minimized and diffusive phenomena are dominant, and in which the nuclei density  $N_0$  is controlled through the refiner content. From these experimental results, we expected to check Hunt's model, and in a more general way, to better understand the underlying physical mechanisms associated with equiaxed dendritic solidification of alloys, and the influence of convection on this type of growth.

## (2) BACKGROUND

Metal alloys normally solidify with dendritic structures. In constrained growth, arrays of columnar dendrites are commonly observed and grow parallel and in a direction opposite to that of heat flow. However, with aluminium alloys used for engineering applications it is frequently desirable to ensure that the cast microstructure has an equiaxed dendritic as opposed to a columnar dendritic morphology. In aluminium the columnar to equiaxed transition is promoted by the addition of inoculants which are termed grain refining master alloys (or grain refiners) [6]. Grain refiners are most commonly Al-Ti-B master alloys. Over the last two decades much work has been done to understand the factors which influence the columnar to equiaxed transition. Hunt [1] proposed to model steady state equiaxed growth in the constitutional undercooled region in front of a columnar array, in order to predict the transition from columnar to equiaxed grain structure as a function of the nuclei density  $N_0$ , and local temperature gradient  $G$  and solidification rate  $R$ . Weinberg and co-workers [2, 3] undertook unidirectional solidification experiments vertically upwards in Sn-Pb and Al-Cu systems, in non steady state conditions, so that  $G$  and  $R$  varied continuously during solidification, to track the CET and check Hunt's model. But they could not verify the Hunt's prediction for inoculated samples, partly due to the low thermal gradients involved. In fact, gravity driven convection may strongly affect both the nuclei distribution and the undercooled region. For this reason, more recent models [4,5,7] try to include these last effects. However, well controlled equiaxed dendritic solidification experiments are needed to provide benchmark data for the testing and refinement equiaxed microstructure evolution models, both in the pure diffusion limit as well as with convection.



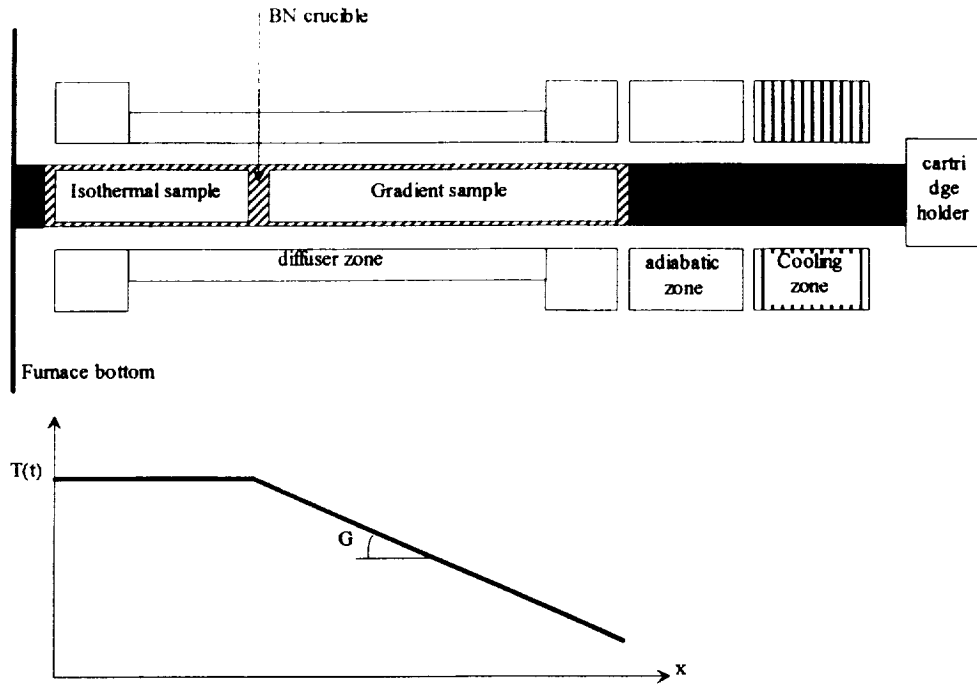


Figure 1 : Schematic representation of LMS-AGHF-ESA 2b experiment.

### Thermal data

Thermal conditions in the gradient samples are analysed by recording time variations of the temperature differences between neighbouring thermocouples of the central capillary. Times corresponding to the passing of the solidification front at the level of each thermocouple are then determined from the breaks appearing on these curves, and the average velocity between thermocouples  $i$  and  $i+1$  is evaluated as :

$$R_i = \frac{x_{i+1} - x_i}{t_{i+1} - t_i}$$

where  $x_i$  is the position of thermocouple  $i$ , and  $t_i$  the passing time of the front at thermocouple  $i$ . The temperature gradient in the liquid ahead the front is then calculated as :

$$G_{Li} = \frac{T_{i+1}(t_i - 2mn) - T_i(t_i - 2mn)}{x_{i+1} - x_i}$$

Values of  $G$  and  $R$  at the beginning and end of solidification are given on Table 2. An example of the overall solidification paths in a  $\log R$  vs  $\log G$  diagram is shown on Fig.5.

### Microstructural examination

Longitudinal sections of solidified rods, taken parallel to the growth direction, were prepared by conventional metallographic procedures. In order to reveal grain morphologies, and to enable equiaxed grain densities to be measured, metallographic sections were anodized with HBF<sub>4</sub> aqueous solution (34% HBF<sub>4</sub> acid in water) at 30 V DC for between 2 and 3 minutes at room temperature. When viewed with crossed polarizers in an optical microscope, grains of different orientations were clearly delineated. Grain density measurements were performed only on those parts of samples that were found to have a fully equiaxed grain morphology. The grain density was evaluated by means of image processing softwares and grains counting methods based on stereology [8, 9].

#### (4) EXPERIMENTAL RESULTS

##### 4.1 Isothermal samples

Typical grain structures formed in isothermal samples under microgravity and on the ground are

shown in the longitudinal sections of Fig.2a and b. Average grain densities measured on the different isothermal samples are given on Table 2.

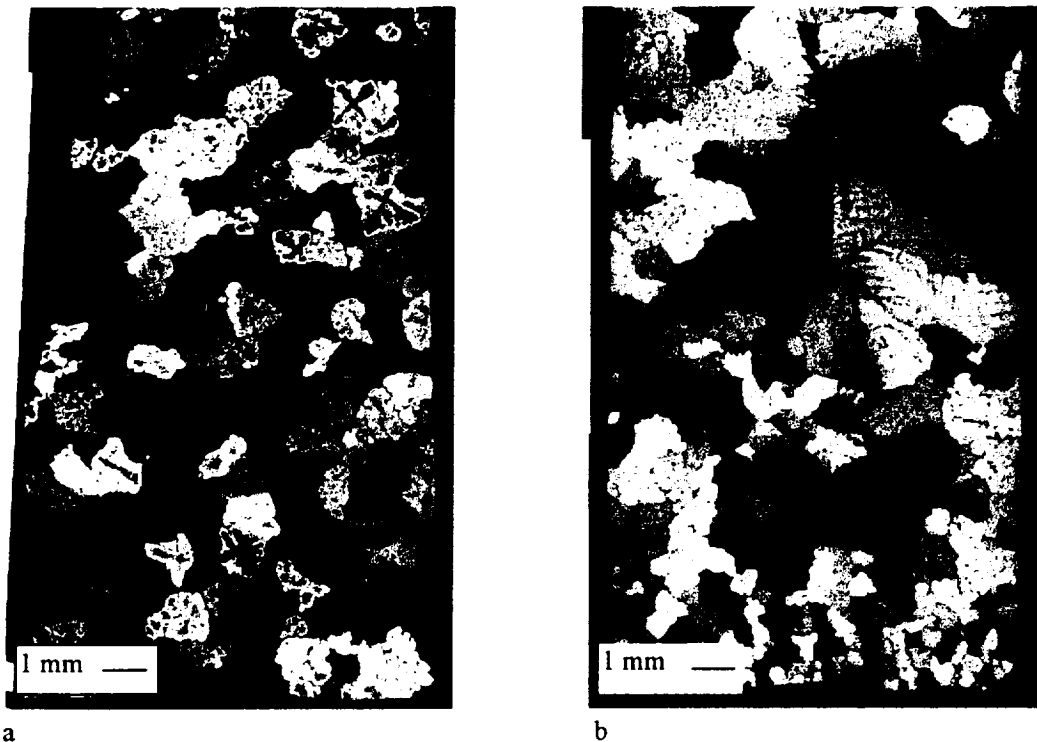


Figure 2 : Optical micrograph of an anodized microstructure viewed under polarized light showing a longitudinal section of : a) FM1 microgravity isothermal sample, with a regular equiaxed structure, b) GM2 ground based isothermal sample, with a strong settling effect.

Sample	$N_0$ (part./mm <sup>3</sup> )	Initial thermal conditions $G(K/cm)$ - $P(cm/s)$	Final thermal conditions $G(K/cm)$ - $P(cm/s)$
--------	--------------------------------	-----------------------------------------------------	---------------------------------------------------

## 4.2 Gradient samples

Microgravity gradient samples FM1 and FM2 show a continuous transition from an anisotropic structure at the beginning of solidification (Fig.3) towards a fully equiaxed microstructure at the end of solidification (Fig.4a). Indeed, the interdendritic segregated regions are found to be elongated and preferentially oriented in the direction of the temperature gradient in the first part of the sample (Fig.3a), and this effect progressively disappears along the solidification direction. This anisotropy is however not reflected in the grain structure itself, which shows no elongation in the solidification direction (Fig.3b). One can only remark a tendency for the grain boundaries to be either parallel to the temperature gradient, or nearly perpendicular to it. Eutectic inclusions are preferentially concentrated along the first type of boundaries. These inclusions form dihedral angles at the intersection of perpendicular boundaries (Fig.3c). In the regions where the grain boundaries are not filled with eutectic, small aligned  $\text{Al}_2\text{Cu}$  platelets are observable (Fig.3d). In presence of excess Ti (FM1 sample), the equiaxed region at the end exhibits smaller dendritic grains.



Ground based GM1 and GM2 samples exhibit slightly different grain structures, due to their different Ti level. The GM1 sample (without excess Ti) is fully columnar, except at the end, where few equiaxed grains appear, mainly on the periphery of the sample (Fig. 4b). In presence of excess Ti (GM2 sample), a sharp transition from purely columnar to equiaxed structure is observed.



## 5.2 Gradient samples

In order to interpret the microstructures observed in the microgravity and ground gradient samples, we will first briefly recall the accepted description of the columnar-equiaxed transition.

*The model of the columnar-equiaxed transition :*

Considering the nucleation and growth of crystals inside the liquid ahead an already formed solidification front (columnar front), and supposing that both the nucleating particles and the growing crystals do not move, three different situations have to be distinguished :

- if equiaxed grains cannot nucleate, i.e. if the constitutional undercooling ahead the columnar front is smaller than the nucleation undercooling, a purely columnar structure is expected ;
- if equiaxed gains can nucleate and grow enough to stop the advance of the columnar front, a fully equiaxed structure will result ;
- at last, if the equiaxed grains do not fill completely the space before being reached by the columnar front, then it is admitted that they will be overgrown by it, so that a mixed columnar-equiaxed structure should be obtained. Let us remark that this presupposes that, due to a selection mechanism associated with the relative cristallographic orientation of the grains, growth of the former columnar grains is preferred to that of the new impinged grains.

A simple model has been proposed by Hunt [1] to predict the conditions for transition between these different microstructures. The main assumptions of the model are the following :

- stationary state is considered, corresponding to the situation of directional solidification in a Bridgman furnace ;
- equiaxed nucleation is possible only in the undercooled region, ahead of the columnar front ; there is no convection, and the equiaxed grains cannot be shifted out of the undercooled region.
- columnar undercooling  $\Delta T_C$  is given as follows :

$$\Delta T_C = \left( \frac{RC_0}{A} \right)^{1/2}$$

R is the columnar dendrite tip velocity,  $C_0$  is the wt.% alloy composition.  $A = -[D/8m (1-k)\Gamma]$  where D is the diffusion coefficient of solute in the liquid, m is the liquidus slope of the phase diagram, k is the equilibrium distribution coefficient and  $\Gamma$  is the Gibbs-Thomson coefficient. In this expression, the  $DG/R$  contribution is neglected.

Briefly, a transition from a mixed to a fully equiaxed microstructure is predicted when :

$$G_L < 0.617 N_0^{1/3} \left[ 1 - \left( \frac{\Delta T_N}{\Delta T_C} \right)^3 \right] \Delta T_C$$

where  $G_L$  is the temperature gradient in the melt,  $N_0$  the number of nucleating sites per unit volume, and  $\Delta T_N$  is the nucleation undercooling. Hunt also considers that the structure becomes practically fully columnar if the volume fraction of equiaxed grains becomes lower than an arbitrary limit. The corresponding transition occurs when :

$$G_L > 0.617 (100 N_0)^{1/3} \left[ 1 - \left( \frac{\Delta T_N}{\Delta T_C} \right)^3 \right] \Delta T_C$$

If  $\Delta T_N$  can be neglected compared to  $\Delta T_C$ , the above relations simplify as follows :

$$G < 0.617 N_0^{1/3} \left( \frac{V C_0}{A} \right)^{1/2} \quad \text{and} \quad G > 0.617 (100 N_0)^{1/3} \left( \frac{V C_0}{A} \right)^{1/2}$$

*Comparison with our space results :*

In our experiment, a preferential growth of the grains in the direction opposite to the heat flux is evidenced by the elongation of the interdendritic segregated regions. But, contrarily to the theoretical expectations, one cannot distinguish two different categories among the grains and none of them appears elongated. A similar trend was observed in the previous MIR experiment with a higher refiner content. But, in the present case, the elongation length of the segregated regions appears even larger than the characteristic dimension of the grains. This can only be explained by a motion of the grain boundaries behind the front. Such a motion of the transverse grain boundaries is possible since they generally did not contain residual liquid (as evidenced by the absence of a eutectic layer). On another hand, the presence of fine Al<sub>2</sub>Cu precipitates along all the boundaries attests that this motion occurred above the eutectic temperature. Finally, a consistent description of the formation of the observed grain structure would be as follows : A large density of more or less elongated grains would initially be formed because, due to the absence of a sharp selection mechanism, new impinged grains would grow as well as the older ones. Then, grain boundaries which become free of residual liquid might start moving, thus leading to a more stable isotropic arrangement of the grain structure. Thus, the above microstructure will be referred to as "recrystallized" in the following.

According to our interpretation, the transition between our recrystallized microstructure and the fully equiaxed one should correspond to the equiaxed-mixed transition of Hunt's model. In order to compare the observed conditions of the transition with the ones predicted by the model, we proceeded in the following way. Due to the low Ti levels of interest, viz 0.001-0.01 wt.%, we have neglected the growth restriction effect (the product  $m(1-k)$  is large for Ti in molten Al [10]), and we have considered our alloys were strictly binary. Thus, we have taken for A the experimental value given by Hunt [1],  $A = 300 \mu\text{m}\cdot\text{s}^{-1}\cdot\text{wt}\% \cdot \text{K}^{-2}$ . As Ziv and Weinberg did [3], we have neglected the  $\Delta T_N$  term before  $\Delta T_C$ .

The isothermal samples were expected to solidify in an equiaxed way, to give us the number of grains per unit volume, and thus the nuclei density  $N_0$ , with the Hunt's assumption where each equiaxed grain is associated with a nucleation event. Grains counting methods based on stereology give more accurate value for the grain density, than estimation from grain size measurements, due to the dendritic form of the grains, and the polydisperse grain distribution. This density, considering the Hunt's model, leads to the construction of equiaxed, mixed and columnar fields on a  $\log(G)$ - $\log(R)$  diagram. Thanks to thermal data, the construction of the « solidification paths » of each experiment was made possible, as illustrated on Fig.5.

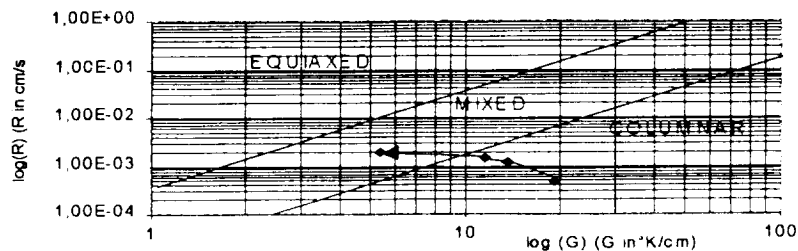


Figure 5 : Plot of growth velocity, R, against temperature gradient, G, showing the predicted columnar and equiaxed regions for GM1 sample, with the experimental solidification path.

It permitted to establish the structures expected by Hunt and compare with our experimental results. This comparison is summarized in Table 3.

Sample	observed grain structure	predicted grain structure
FM1	recrystallised-equiaxed	columnar-mixed
FM2	recrystallised-equiaxed	columnar-mixed
GM1	columnar-equiaxed	columnar-mixed
GM2	columnar	columnar-mixed

Table 3 : Comparison between the observed and predicted grain structures

It appears that our microgravity samples are more equiaxed than predicted. Several hypothesis can be made to explain this departure :

- in Hunt's model, the contribution of solute boundary layer built-up ahead the columnar front to decrease its temperature (by around  $DG/V$ ) is neglected. This effect, which is not negligible in the first part of our solidification path, does not change the local undercooling, but increases the extent of the undercooled region, and thus gives more time for the equiaxed crystals to grow ;
- taking into account the growth restriction effect of Ti should slightly decrease the A value, and thus shift the predicted transition towards lower velocities and higher gradients. On another hand, no significant difference is observed in this respect between the samples with and without excess Ti.

*Ground samples / the effect of convection on the columnar-equiaxed transition :*

Qualitatively, different complementary factors can be invoked to explain the observed shift of the columnar-equiaxed transition under the effect of convection :

- as already evidenced on isothermal samples, the settling of nucleating particles causes an accumulation in the lower stagnant parts and a depletion of  $N_0$  elsewhere ;
- in addition, part of the growing equiaxed crystals may be swept away from the front ;
- at last, the solute built-up ahead the front, and thus the corresponding contribution to the front undercooling, are reduced, which leads to a decrease of the extent of the undercooled region.

The first factor can be taken into account at first order in the frame of Hunt's model by deriving  $N_0$  from the average grain density measured in isothermal samples (Table 2). In this way, a rough agreement is found with our ground experiments, which might be explained by the fact that negligence of solute built-up is better justified in this case.

## (6) CONCLUSIONS

The present microgravity experiment has for the first time shown a continuous transition from a purely equiaxed to an anisotropic solidification microstructure as a function of solidification rate and the local temperature gradient at the front. The conditions for the transition have been found to somehow depart from the ones predicted by the simple model of Hunt which in particular neglects the influence of solute built-up ahead the front. In addition, the aspect of the anisotropic microstructure is not the same as anticipated in the model. This might be due to the fact that for our experimental conditions, there was no strong selection mechanism operating.

By comparison, a very different microstructure is obtained in the corresponding ground references. This is mainly the result of the important settling of the nucleating particles occurring during the long stay in the liquid state inherent to the thermal profile presently applied. However this single effect can hardly explain the abrupt character of the transition between zones with very

large columnar grains and purely equiaxed zones. A possible other factor is the motion of the growing equiaxed crystals relative to the advancing columnar front. This last point is a topic for our next proposed experiment in AGHF, which will focus on the morphology of the equiaxed grains themselves.

## ACKNOWLEDGEMENTS

The authors are greatly indebted to the European Space Agency and specially to J. Stroede. The financial and technical support of the Centre d'Etudes Spatiales is also gratefully acknowledged. Special thanks are given to H. N'guyen Thi for his support at the LMS mission, as well as to D. Buscoz and J.E. Mazille for the Image Analysis.

## REFERENCES

- [1] J.D. Hunt, *Mater. Sci. and Eng.* **65**, 75 (1984).
- [2] R. B. Mahapatra and F. Weinberg, *Metall. Trans.* **B18**, 425 (1987).
- [3] I. Ziv and F. Weinberg, *Metall. Trans.* **B20**, 731 (1989).
- [4] C. Beckermann and C.Y. Wang, *Annual Rev. Heat transfer*, vol. VI, ed. C.L. Tien (1995).
- [5] M. Rappaz et al., *Materials Science Forum* vols. **217-222**, 7 (1996).
- [6] D.G. Mc Cartney, *Int. Mater. Rev.* **34**, 247 (1989).
- [7] C.Y. Wang and C. Beckermann, *Met. and Mat. Trans.*, Part I to III (1996)
- [8] F. Botalla, DEM internal Report n° 09/97, CEA Grenoble, 1997
- [9] D. Buscoz DEM internal Report n° 10/97, CEA Grenoble, 1997
- [10] M. Johnsson, L. Backerud and G.K. Sigworth, *Metall. Trans.* **A24**, 481 (1993).

## SUMMARY OF THE LMS-AGHF-ESA 2b EXPERIMENT

In the case of directional solidification of inoculated alloys under diffusive transport conditions, the transition from columnar to equiaxed grain structure is predicted to occur continuously through intermediate mixed structures, as a function of the nuclei density  $N_0$ , temperature gradient  $G$  and solidification rate  $R$ . On the ground, gravity driven convection affects these three parameters. For this reason, recent models try to include convective effects. However, in order to assess the models, experiments able to separate convection from the other mechanisms involved are still needed.

With this aim in view, we performed a series of experiments under reduced gravity (EUROMIR 95 and LMS 96) where Al-4wt.%Cu alloys refined at different levels (2 to 50 ppm B, and 10 to 250 ppm Ti) with Al-5Ti-1B master alloys, were unidirectionally solidified with continuously decreasing temperature gradient  $G$  and increasing rate  $R$ . Nearly isothermal samples from the same batch were also solidified in parallel, to give the reference purely equiaxed microstructure. Reference ground based experiments were also performed in identical thermal conditions with different orientations relative to gravity. In the present work, the results of the LMS experiments are analysed.

In the samples solidified in microgravity under nearly isothermal conditions, the refiner is found to operate, even for the case of the low Ti content (10ppm). This result shows that there is no significant fading of the efficiency of the refiner particles during their long stay into the liquid (4 hours), and that, if a lower limit of excess Ti necessary for heterogeneous nucleation on the  $TiB_2$  particles exists, it should be very low. However, the grain size is significantly smaller in the sample with 100ppm Ti. This may be due to an increase of the number of efficient nucleation sites and/ or a contribution of the Ti content in the liquid to slow down the growth of the equiaxed grains.

Comparatively, the grain structure in the ground samples is strongly influenced by the settling of refiner particles towards the bottom. This settling is however not complete due to the slight mixing

by natural convection.

Samples solidified under varying  $G$  and  $R$  in microgravity show for the first time a continuous transition from a purely equiaxed to an anisotropic solidification microstructure as a function of solidification rate and the local temperature gradient at the front. The conditions for the transition are found to somehow depart from the ones predicted by the simple model of Hunt which in particular

Advanced Gradient Heating Facility (AGHF)

## Effects of Convection on Interface Curvature during Growth of Concentrated Ternary Compounds

Principal Investigator:

Dr. Thierry Duffar  
DEM/SES  
Grenoble, France



DTA - CEREM  
DÉPARTEMENT D'ÉTUDES DES MATÉRIAUX

Fiche d'Action GRAMME

*Service de l'Union Chimique Matériau*

Grenoble, le 25 juillet 1997

COMpte RENDU SPCM n° 15/97

LMS One year science review

PRELIMINARY RESULTS OF THE  
AGHF ESA-8 EXPERIMENT

N. DUHANIAN, T. DUFFAR (Principal Investigator), J. ABADIE

Liste de diffusion du CR. SPCM n° 15/97 du 25 juillet 1997

Conseiller Scientifique M2RI	M. FAVIER
M2RI/DEM/Dir (1 seul ex.)	MM. LEMOINE AUBERT
DOC/DEM	
M2RI/DEM/SPCM	MM. ABADIE CAMEL DUFFAR Mlle DUHANIAN Mme DUPOUY M. GARANDET Mme KERNEVEZ MM. NABOT PRAIZEY SANTALLER WARIN
Conseiller Scientifique	M. DESRE
C.N.E.S./Paris	MM. BONNEVILLE ZAPPOLI Mme LEON
NASA-MSFC, Huntsville	M. DOWNEY
Univ. Autonoma Madrid	M. DIEGUEZ
ESA/ESTEC	M. STRÖDE MM WALTER, MINSTER
CNES Toulouse/CADMOS	M. DESROCHES

Page de garde + Résumé + Liste de diffusion

M2RI/DEM/SGM	MM. MORET DANROC ROBERT BLOCH
M2RI/DEM/SPCM/DIR	Mme MERMILLIOD
M2RI/DEM/SPCM/LSE	Tous A1 et Thésards
M2RI/DEM/SPCM/LSC	
M2RI/DEM/SPCM	

## RESUME

L'expérience spatiale LMS-AGHF-ESA8 est dévolue à l'étude de la solidification des alliages concentrés. C'est un domaine qui souffre simultanément de l'absence de description théorique rigoureuse des phénomènes physiques mis en jeu et d'un manque d'expériences soignées pour les valider.

Nous décrivons le dispositif expérimental et les paramètres de l'expérience, choisis pour en optimiser les résultats. L'alliage retenu est le pseudo-binaire semiconducteur GaSb-InSb, pris comme matériau modèle.

Les premiers résultats expérimentaux, qui restent à compléter par des mesures plus approfondies, permettent de tirer des conclusions dans deux domaines :

- Du point de vue ségrégations chimiques, on a mis en évidence dans l'échantillon spatial une homogénéisation inattendue du liquide tout au long de la solidification. Ce phénomène ne rentre pas du tout dans le cadre de notre compréhension actuelle de la solidification des alliages concentrés.
- Sur le plan des interactions cristal-creuset, le phénomène de démouillage, consistant en un décollement de l'échantillon par rapport au creuset, a été quantifié pour la première fois. Les résultats

---

obtenus sont en bon accord avec nos derniers développements théoriques sur le sujet.

## ABSTRACT

The space experiment LMS-AGHF-ESA8 was devoted to studies on the solidification of concentrated alloys. Indeed, the knowledge in this field suffers simultaneously of a lack of theoretical description of the physical phenomena involved and of clear experiments to validate them.

We describe the experimental set-up and the experimental parameters chosen in order to optimize the results. The alloy used is the pseudo-binary semiconductor GaSb-InSb, taken as model material.

The first results, still to be confirmed by more in depth measurements, lead to conclusions in two domains :

- The chemical segregations in the flight sample have shown an unexpected homogenization of the liquid all along the solidification. This phenomenon does not agree with the present understanding of the solidification of concentrated alloys.
- The crystal-crucible interactions, leading to detachment under microgravity conditions, have been quantified for the first time. The results are in good agreement with our theory on the subject.

## ACKNOWLEDGMENTS

This experiment has been supported by the ESA, the GRAMME agreement between CEA and CNES and the Spanish Ministry of Research. The development and exploitation of this experiment have only been possible due to the great efforts of a number of people involved at various stages. The PI's would like to thank all of them for their efforts :

C. Marin and P. Dutta for the preparation of the feed and seed materials.

J. Abadie for taking care of the cartridges' development, design and integration.

J.P. Pissard, S. Cantaloup and the teams in SOTEREM and CNES for the industrial integration of the cartridges.

A. Desroches, G. Begnini, and the whole CADMOS team for their help during the flight and ground experiments.

B. Desaunettes and P. Vedrenne, EPSILON, for their help in numerical simulation of the thermal field in the cartridges.

The ESA team at the POCC, with a special mention for J. Ströede , head of the AGHF project at ESA.

N. Duhanian for taking care of the ground reference experiments, for the processing of the samples and analysis of the experimental results.

But our best regards will be for H. Ben Aïm, for her constant help and support, and Adèle ...

## 1 SCIENTIFIC OBJECTIVES

The ESA8 experiment is essentially devoted to the study of the solidification of concentrated alloys. When an alloy is melted then solidified back, a number of phenomena are occurring, which has an impact on the quality of the resulting solid. For example, there are several growth regimes during solidification that lead to very different structures of the sample: the first stage is characterized by a smooth solid/liquid interface; when the growth rate is increased, the interface becomes wavy and, at highest rate, totally disturbed. We have restrained our experiment to the first stage.

The shape of the solid/liquid interface and the chemical segregations of the components of the alloy have a large influence on the final quality of the sample. These phenomena are now rather well understood in the case of diluted alloys (i.e. when the chemical composition has no sensitive effect on the physical parameters of the sample, such as density or melting temperature) but there is a lack of both theory and experiments in the case of highly concentrated alloys [1].

Indeed, the large number of physical phenomena involved make the problem very complicated:

- Heat transfer in the liquid and solid phase, including release of latent heat at the interface.
- Hydrodynamical movements in the liquid that are due to differences in temperature or in chemical composition. The resulting variations of density interact with the gravity field and generate movements.
- Chemical segregations during solidification due to the fact that the solidified solid has not the same composition than the liquid: some components of the alloys stay in the remaining liquid rather than being incorporated in the solid.

In diluted alloys, these three phenomena are well decoupled (the thermal field induces movements that induce chemical species transport) and the problem is rather simple (but it took more than thirty years to get a satisfactory model!). In concentrated alloys, there is feedback between the phenomena (chemical field induces movements and modifies thermal properties, especially melting temperature) which makes the problem much more complicated.

The purpose of the experiment is to quantify the effect on solidification of variations in the external thermal field (by varying the crucible material) and in the gravity level (by comparison between space and ground experiments) by measuring:

- The temperature distribution around the sample.
- The interface shape along the growth process.
- The chemical segregations in the resulting solid.

Another, totally independent, objective of the experiment is to study the phenomena of dewetting. This denotes a detachment of the sample from the crucible, which is commonly observed when semiconductor materials are solidified under microgravity conditions [2, 3] even though it is never observed on earth.

## 2 EXPERIMENT PARAMETERS, DEVELOPMENT AND PROGRESS

The alloy is a mixing of 20% (molar) of InSb and 80% of GaSb. These two compounds are semiconductors that can be mixed in any proportion in the solid and liquid states and then the system can be considered as binary. Antimonides are the less toxic semiconductor compounds and furthermore they melt at the lowest temperature (530°C for InSb and 710°C for GaSb). This makes them good candidates for a space experiment where safety concerns are mandatory and thermal energy restricted. They are well known to show the dewetting phenomenon.

The InSb is heavier than GaSb and is rejected in the liquid. It is then expected that it stabilizes the convective motion of the liquid close to the interface when the alloy is solidified vertically on earth and that is why it has been chosen as the « solute ». The concentration of 20% corresponds to the maximum difference between the solidus and liquidus lines of the pseudo-binary phase diagram. The physical properties of these materials are very well known, including wetting properties on the crucibles (wetting is of importance in the detachment matter).

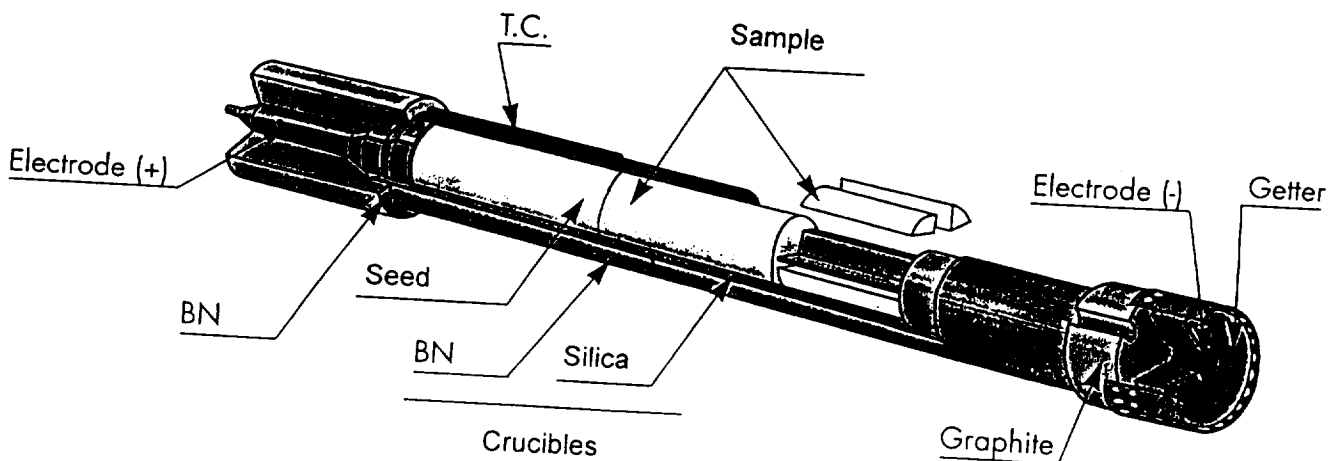


Fig 1: Sketch of the experimental set-up.

To avoid undercooling of the sample, a « seed », which is not melted and is used as initiator of the growth, is placed at the cold side of the sample. Because the experiment is not focused on structural quality, the seed is not a single crystal. Seeds and feed materials have been prepared from pure (6N) In, Ga, Sb and Te. The preparation by itself is a complicated task that led to a specific publication [7].

In order to act on the interface curvature during the growth, two crucibles are used. One is made in quartz, with a very low thermal conductivity that gives interfaces with a very low curvature. The second one is in boron nitride (BN) which gives strong interface curvatures. The inner diameters of the crucibles were measured with a precision of a few micrometers, for subsequent comparison with the external diameter of the solidified samples. Both crucibles don't conduct electricity. This is of importance because the investigation on the interface curvature is made by applying electrical pulses to the sample at regular intervals. By this way the Joule effect and the Peltier effect generate heat close to the interface and disturb the growth. This disturbance can be revealed by subsequent cutting, polishing and etching of the sample : the shape of the interface at the moment of the pulse is materialised by a thin line visible on the polished, etched surface. By measuring the distance between two lines, and knowing the time between the two electrical pulses, it is also possible to calculate the growth rate. The parameters of the Peltier pulse marking are: duration 800 ms, amplitude 18 A and they are sent every ½ hour. It is necessary to dope the alloy with Te ( $10^{19}$  to  $10^{20}$  at/cm<sup>3</sup>) in order to get a good etching and demarcation of the interfaces. The electrical current enters the sample by the hot (liquid) side, via a graphite piece and is collected at the cold part by a bronze pincer around the seed. Nine thermocouples are placed all along the crucibles in order to measure in real time the thermal field around the sample.

To avoid pollution of the sample, the experimental set up, which is enclosed in a standard Ta cartridge, is under vacuum. A getter is placed at the hot part in order to pump the remaining gases during the heating of the cartridge.

Given the chemical composition, the growth rate, thermal gradient, diameter and length of the sample are a compromise between several constraints:

- Allocated time for the experiment.
- Avoidance of interface destabilization due to constitutional supercooling (the interface must remain smooth).
- Avoidance of thermal convection due to residual gravity fluctuations during the space experiment.
- Interface curvature must be high enough so that fluctuations are detectable.
- Border effects at the beginning and end of the sample must be avoided.

Taking into account the available theoretical literature on these effects [4-6], the optimal parameters were found:

- Growth rate 1.1  $\mu\text{m/s}$ . This will be the value chosen for the furnace pulling.
- Thermal gradient in the liquid: 60 K/cm.
- Sample diameter 12 mm.
- Sample length: 152 mm plus 63 mm of seed. At least 95 mm of the sample will be solidified under controlled conditions.
- Experiment duration (controlled growth): 24 hours.

In order to optimise the experimental design and the thermal profile, two prototype tests have been performed. A qualification test, including vibrations, has then been performed in order to fix the flight design and parameters. Only minor modifications have been implemented after these tests. The most important was due to the fact that it has been found impossible to identify the Peltier pulse marks when they are sent with a perfect periodicity. A few pulses with an interval of ten minutes have then been put among the  $\frac{1}{2}$  h spaced pulses.

The scientific observations performed on the samples during these preliminary tests have been communicated [8]. They will be emphasized in a most quantitative way for the ground reference test.

During the first attempt to perform the experiment during the flight, a fault corresponding to an open circuit in the Peltier pulse marking electrical circuit was detected by the furnace. The electrical resistance of the Peltier circuit was measured by the crew in the flight model (infinite value, open circuit) and in the spare model (0.6 Ohms). It was then decided to process the spare model for the second attempt. The cartridge has been inserted without problem and the processing (pulling of the furnace) phase began at MET 9/14:02 for 26 hours and 40 minutes: the experiment gained the advantage of been processed during the 11th day of the mission that was a rest day for the crew. Then the gravity disturbances were supposed lower than for a busy day. Figure 2 gives the process parameters of the furnace versus time, as programmed in real time during the flight experiment.

The thermocouples' measurements were analysed directly during the flight. (Excepted TC1 which failed after 2h at high temperature). The interface position versus time, extrapolated from the melting temperature and TC readings, showed a very constant nominal growth rate. The thermal gradients in the liquid were 60°C/cm or higher, as expected.



LMS - AGHF ESA8 - FLIGHT

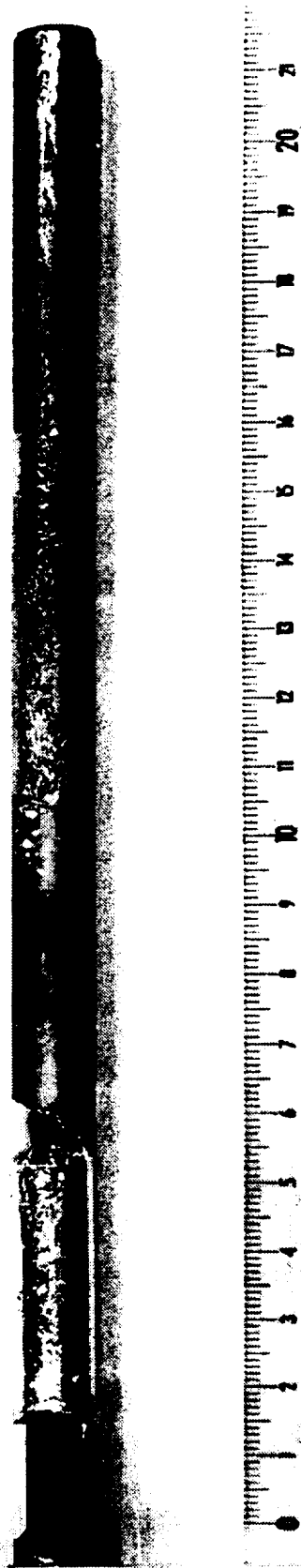


Fig 3: External view of the flight sample. The seed is on the right (between 16 and 21 cm), the BN/SiO<sub>2</sub> junction at 10.5 cm and the bubble can be seen on the left (between 5 and 6 cm).

Vacuum inside the cartridge has been measured at the opening: 10 mbar. These residual gases were not analysed.

The ground reference test has been performed end of November 1996 in the flight model of the furnace, with the same parameters than for the flight, using the flight cartridge initially rejected by the furnace. Every process parameters and observations were nominal and no bubble was observed.

### 3 RESULTS ON CRUCIBLE-SAMPLE INTERACTION

Visual observation of the flight and ground samples shows a clear difference of external aspect in the BN crucible. In the quartz crucible, on the contrary, the aspect is the same. Fig 4 shows the surface morphology of the flight sample in the middle of the BN crucible. Fig 5 shows the morphology at the BN/SiO<sub>2</sub> junction. On the SiO<sub>2</sub> side, the external surface of the sample is a molding of the roughness of the machined crucible, as well as in the case of the ground sample. Fig 6 and table 1 give a profilometer quantification of the surface roughness.

	SiO <sub>2</sub>	BN
Ground	3 μm	7 μm
Flight	3 μm	25 μm

Table 1: Apparent roughness (Ra) of the sample in the two crucibles, compared between earth and space.

Fig 7 and Fig 8 show the variations of the sample external diameter and of the crucible internal diameter (as measured before and, when possible, after the experiment). The results are practically the same for ground and space samples. Due to the measurement method (electronic vernier), the measured diameter for the BN part of the flight sample is taken on the ridges. It can then be inferred that the outer top surface of the ridges touched the crucible wall because there is clear evidence that the ground sample, with the same diameter, touched the crucible. In the case of the flight sample, it can be

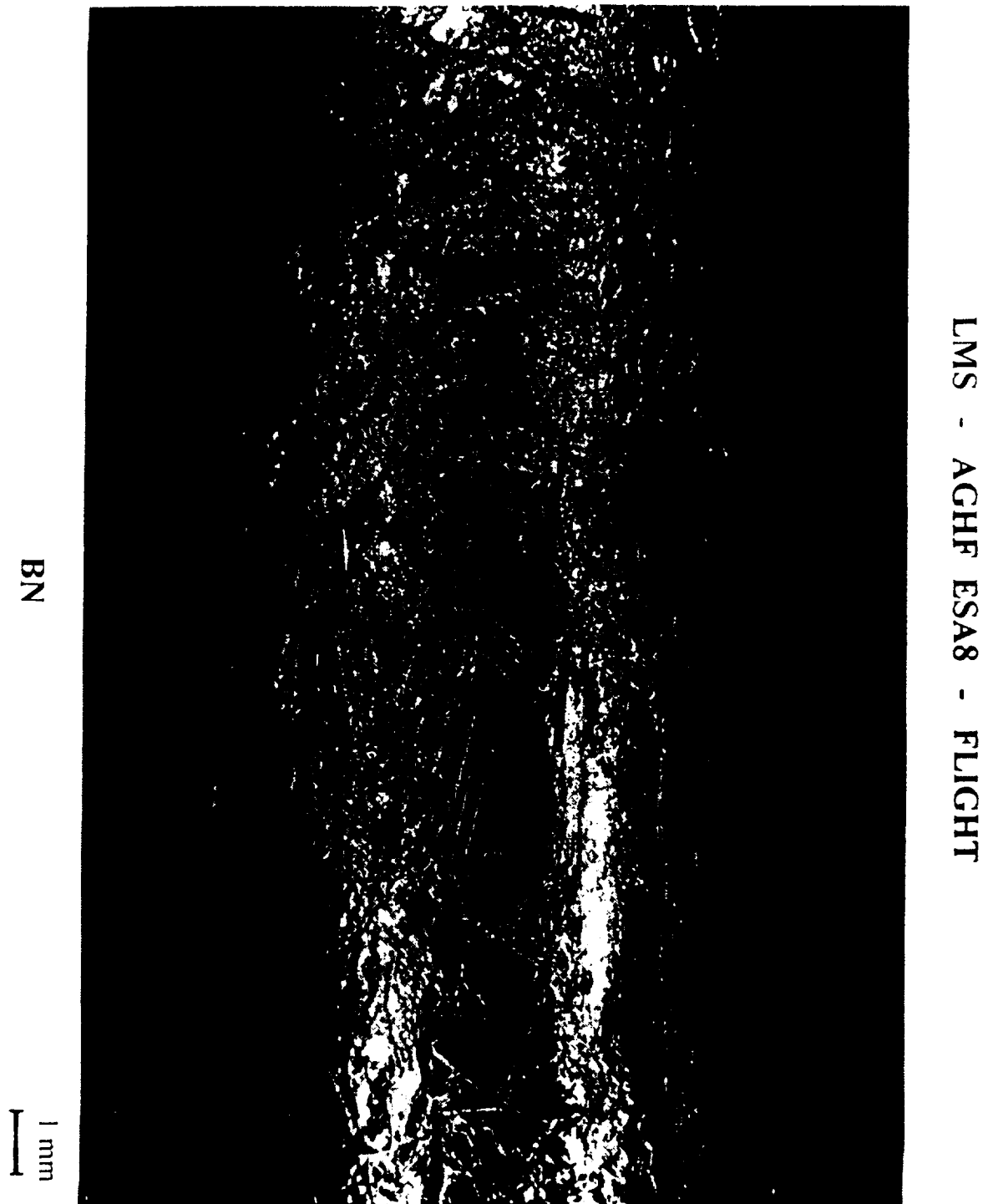
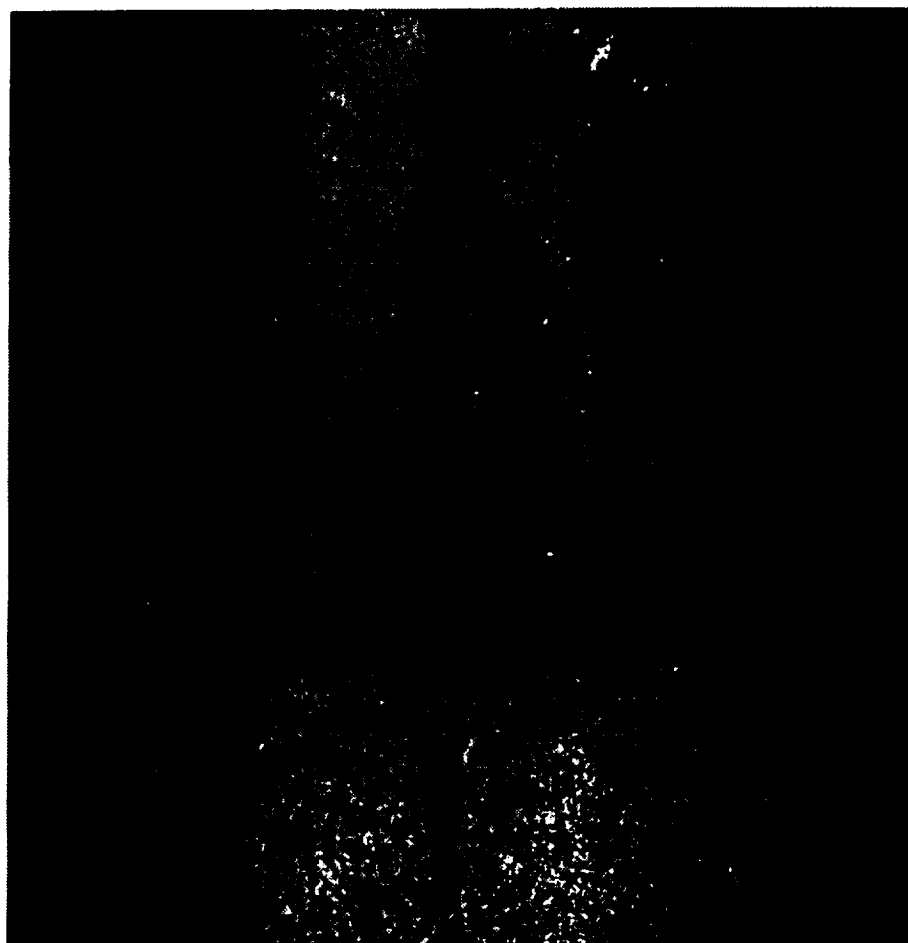


Fig 4: External aspect of the flight sample from the BN crucible

The conclusions of these observations are that the dewetting of the sample occurred only in space for the BN crucible. The sample shows the classical « ridges » on its surface. From the profilometers, the depths of the valleys between the ridges have a mean value of 25  $\mu\text{m}$  with maximum values of 40  $\mu\text{m}$ .

For the three other configurations, the sample was a molding of the roughness of the BN or SiO<sub>2</sub> crucibles. Considering that the contact angle of antimonides on silica is 120° and on BN 135° [9], it can be concluded that the largest contact angle causes de-wetting and the lowest causes sticking. These results are in good qualitative and quantitative agreement with our understanding of de-wetting [2,3].

QUARTZ



LMS - AGHF ESAS - FLIGH

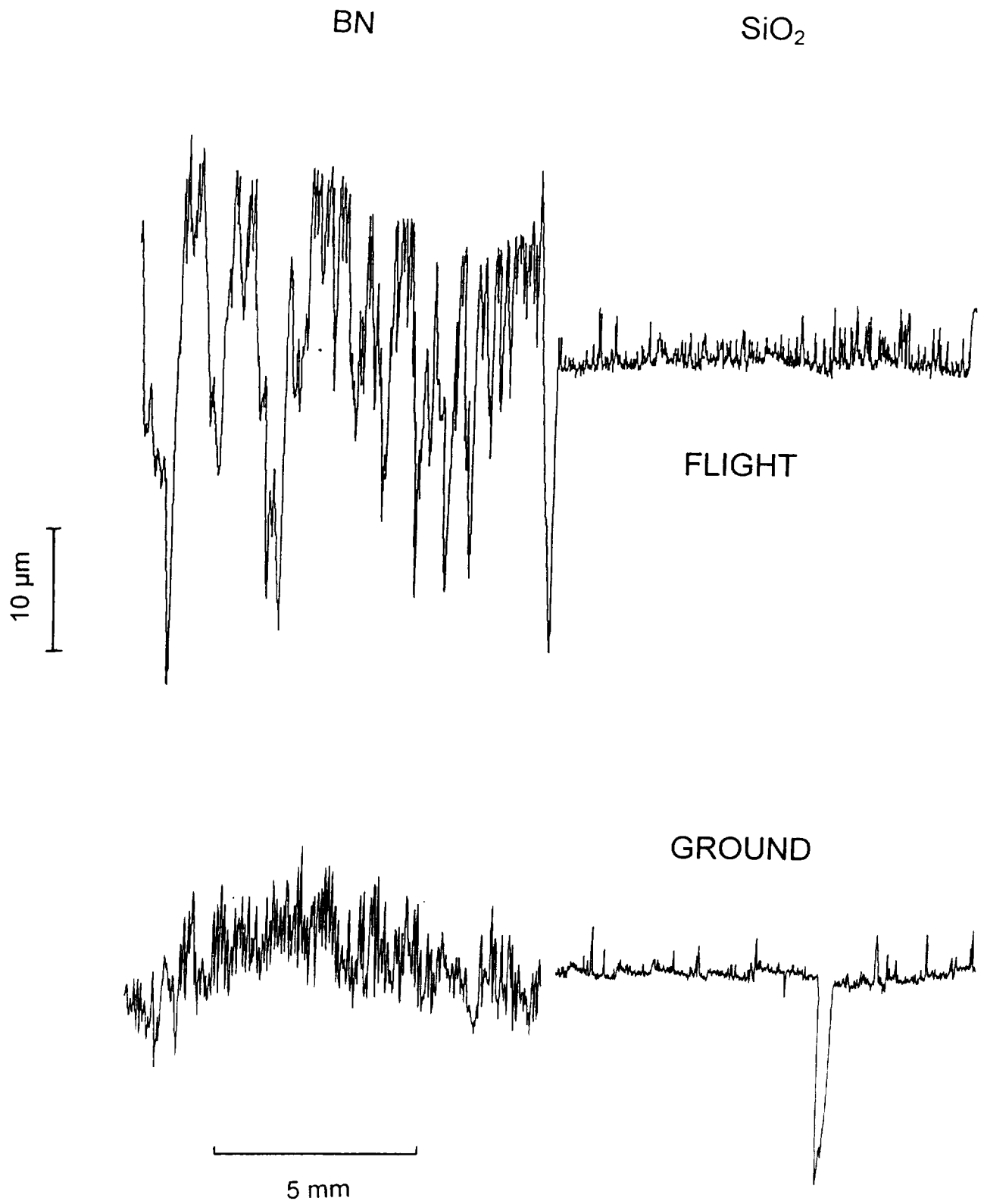


Fig 6: Surface roughness of the flight and ground samples in the BN and SiO<sub>2</sub> crucibles.

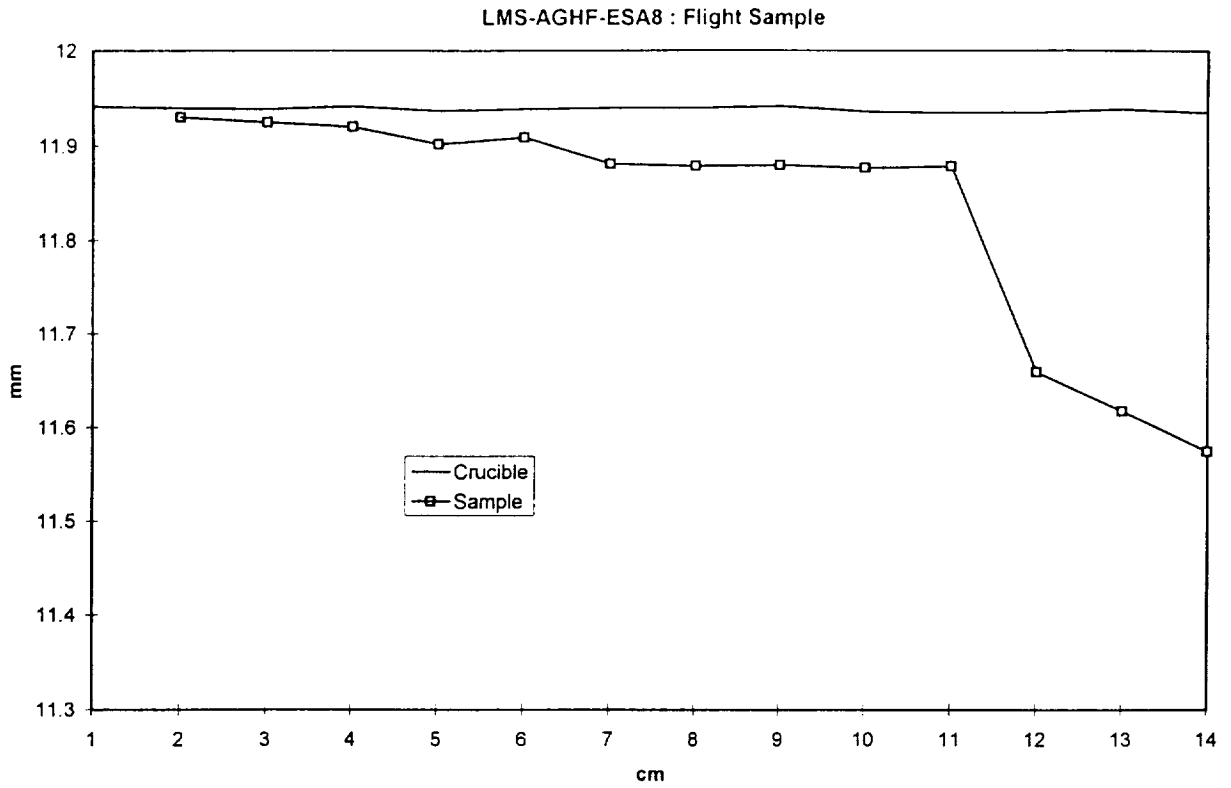


Fig 7: Internal diameter of the crucibles and external diameter of the sample after the flight experiment, versus sample length.

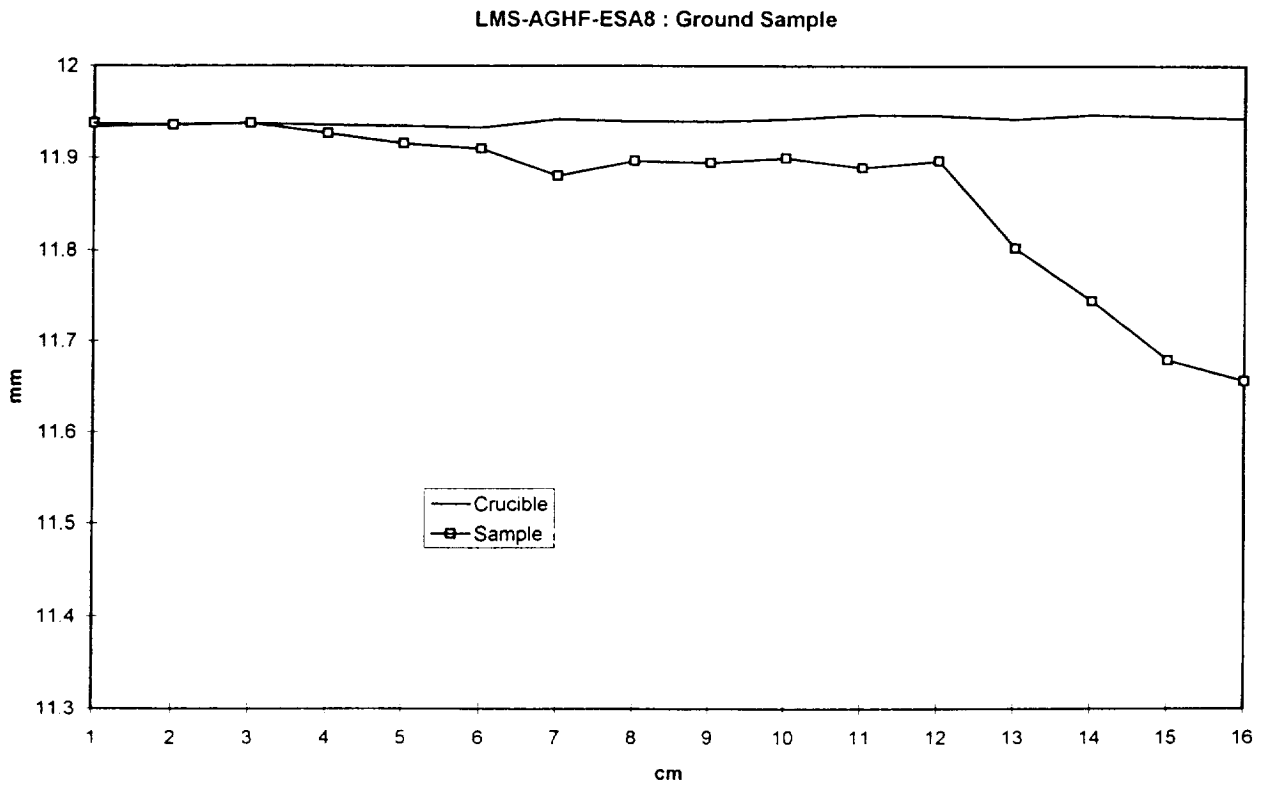


Fig 8: Internal diameter of the crucibles and external diameter of the sample after the ground experiment, versus sample length.



Mullins-Sekerka criteria, because of a too low concentration at this point. The classical destabilisation can be seen at the 10% level, at the end of the sample. Further in depth chemical analysis, especially close to the BN/SiO<sub>2</sub> junction, are needed to have a better insight on the results.

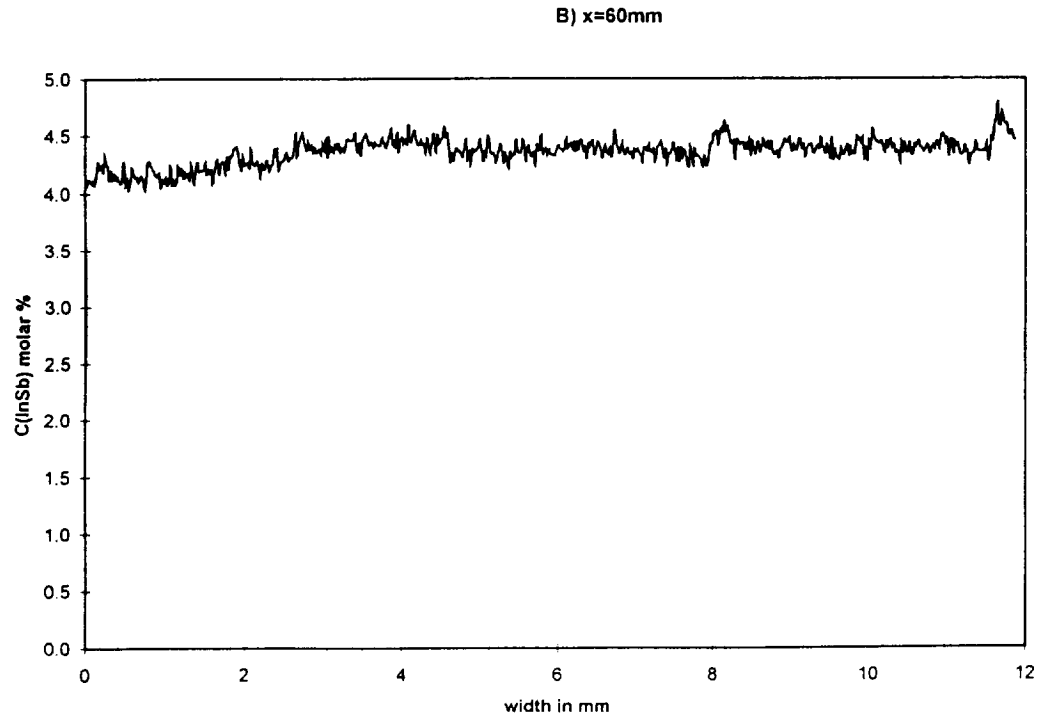
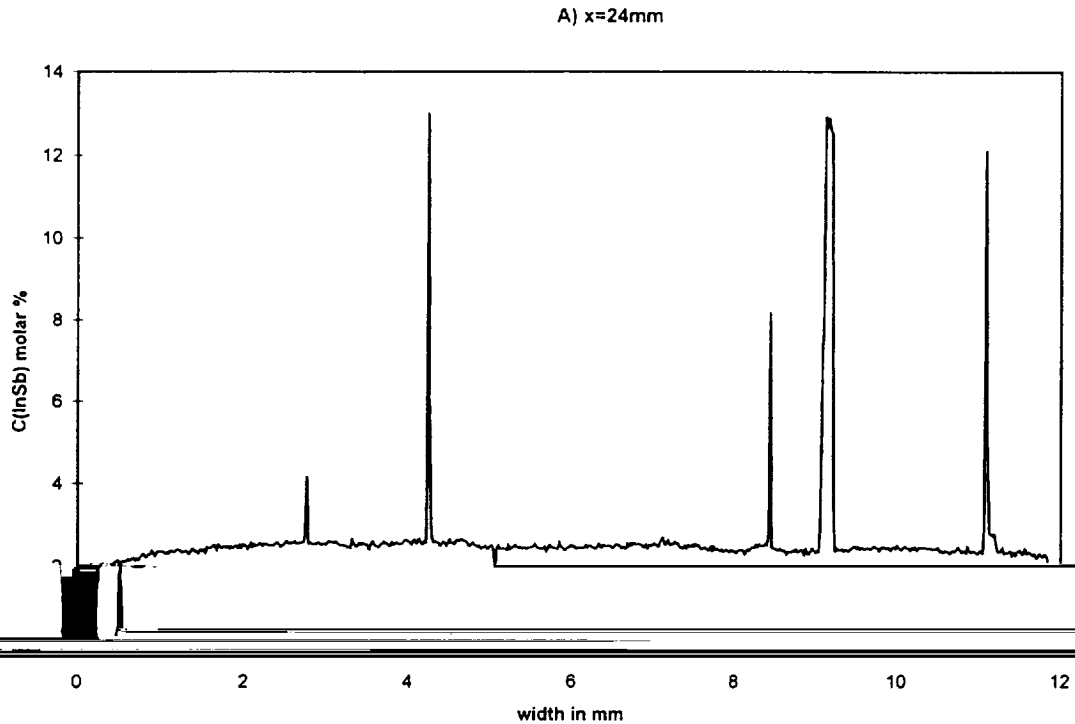


Fig 10: Radial InSb concentration along sample diameter, at the positions A and B.



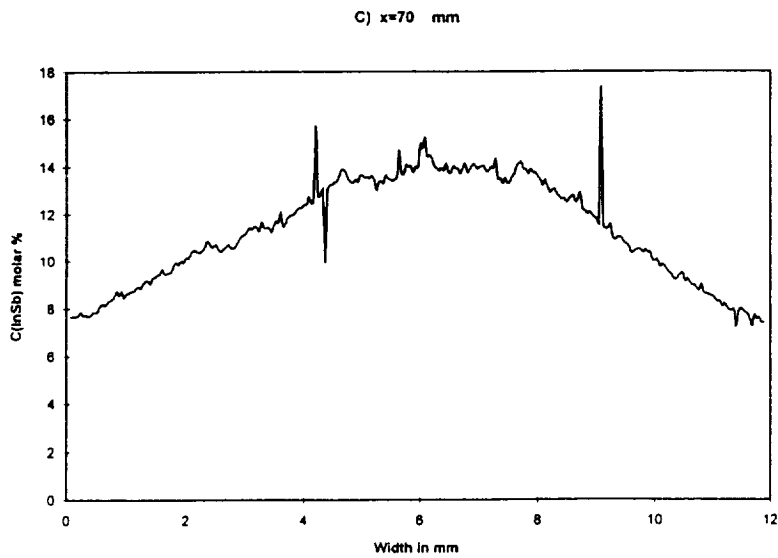
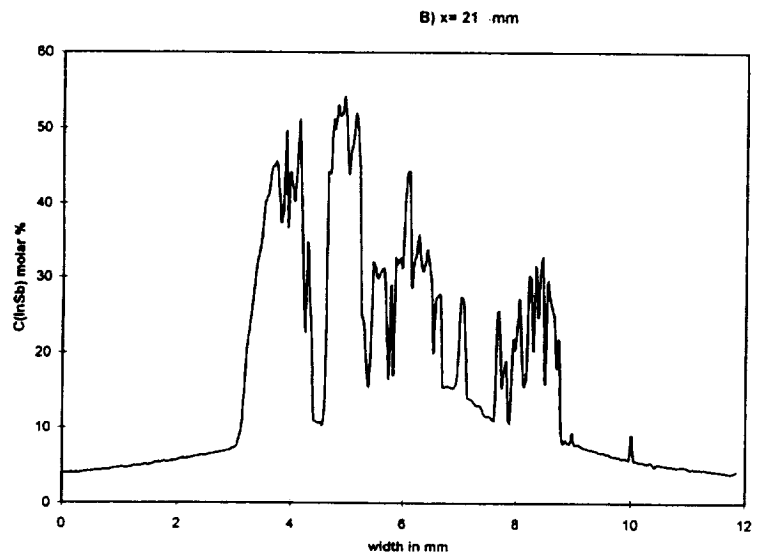
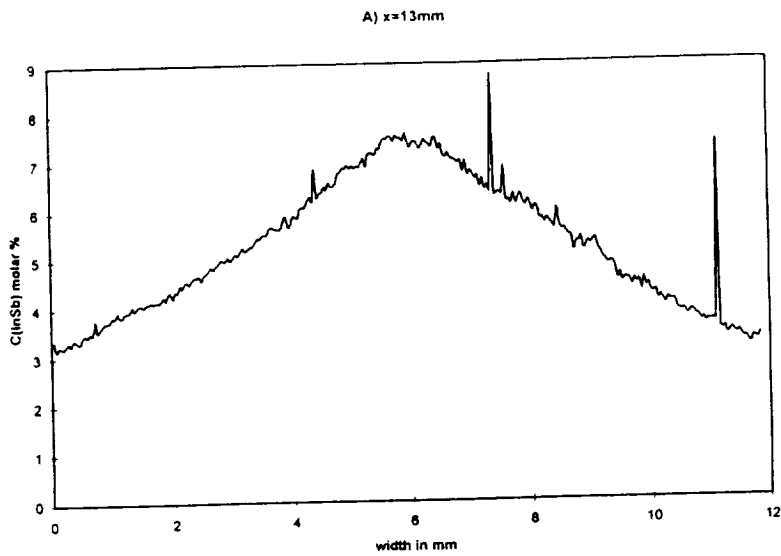


Fig 12: Radial InSb concentration along diameter of the ground sample, at the positions A, B and C.

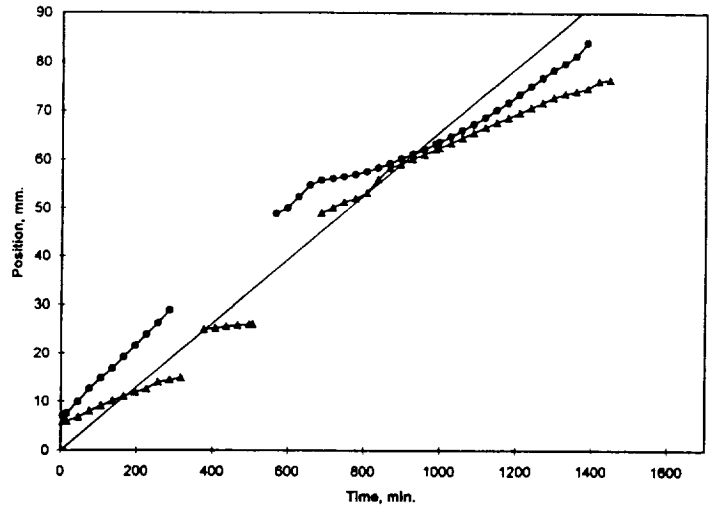
For the ground sample, Fig 11 and 12 give the longitudinal (on the axis) and radial segregations. Fig 13 shows the structure of the sample and the marked interfaces, as revealed by chemical etching. It can be seen that the middle of the sample is destabilized after some distance of growth in the BN and SiO<sub>2</sub>. In between, the quality is rather good. A very qualitative explanation of these observations can be given:

- The initial solid liquid interface is curved, concave when seen from the liquid, due to thermal field.
- When growth proceeds, the InSb is rejected, especially toward the center of the sample (due to the curvature), where the concentration increases (see fig 12-A) and then the melting point decreases.
- This leads to a more curved interface (fig 13) and the process goes ahead with a greater and greater amount of InSb toward the axis.
- Destabilisation occurs (Fig 12-B) when the axial and radial thermal gradients are no more sufficient to stabilise the interface.
- At the junction between the two crucibles, the thermal field in the liquid is highly distorted and this gives a strong thermal convection that mixes the liquid.
- Then the process is repeated in the silica.

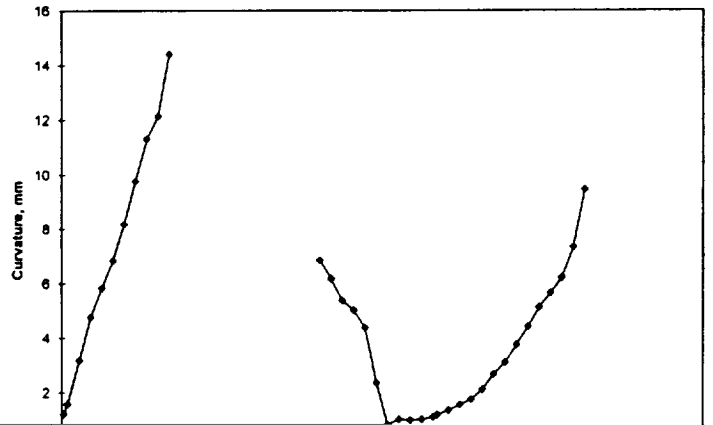
Of course, this is only a very hypothetical explanation and it is necessary to quantify the relative magnitude of thermal convection, solutal damping, increase of interface curvature, etc., in the transient process in order to validate it. Because of the very complicated, highly coupled non linear nature of the problem, only a full numerical simulation taking into account all the thermal, hydrodynamical and chemical phenomena can be used for this purpose.



ESA8-ground sample : Interface position in the middle and on the side  
Straight line : furnace position



ESA8-Ground sample : Interface curvature.



## 5 CONCLUSION

This experiment has given important results concerning two major effects of microgravity in semiconductor growth:

- The de-wetting phenomenon has been quantified in terms of sample roughness and diameter. It has been shown that the contact angle of the liquid on the crucible gives de-wetting when it is high and sticking when it is lower. The measurements and observations are in good agreement with our understanding of the phenomena.
- Chemical segregation analyses have shown that, under less than  $10^{-5} g_0$  residual accelerations, a full mixing of the rejected solute in the remaining liquid is observed close to the interface. This result cannot be explained with a simple estimation of the leading convective forces.
- Segregations observed on earth show complicated behavior which will necessitate a detailed global numerical simulation to assess our qualitative description. It is hoped that the quality of the experimental results is good enough to validate, or invalidate, the results of the simulation.

Further work on this experiment concerns full analysis of the thermal data, taking into account the

BIBLIOGRAPHY (ref. 7, 8 and 12 are directly related to the ESA8 experiment)

- [1] « Handbook of crystal growth », D.T.J. Hurle Editor, North Holland, 1993
- [2] T.Duffar, I.Harter, P.Dusserre Journal of Crystal Growth, Vol 100 (1990) pp 171-184
- [3] T. Duffar, P. Boiton, P. Dusserre, J. Abadie, J. Crystal Growth, under press.
- [4] S. Corriel, F. Sekerka, J. Crystal Growth, 46(1979) 479-482
- [5] J.P. Garandet, J. Crystal Growth, 125 (1992) 112-120
- [6] C. Barat, Ph-D Thesis, Univ. de Rennes, 1995
- [7] C. Marin, P. Dutta, E. Dieguez, P. Dusserre, T. Duffar, J. Crystal Growth, 173 (1997) 271-276
- [8] N. Duhanian, T. Duffar, J. Abadie, C. Marin, E. Dieguez, M. Chaudet, 5èmes journées de la matière condensée, Soc. Fr. Physique, Orléans, 28-30 Aout 1996
- [9] I. Harter, P. Dusserre, T. Duffar, J.P. Nabot, N. Eusthatopoulos, Journal of Crystal Growth, Vol 131 (1993) pp 157-164
- [10] S. Lehoczky, F.R. Szofran, D.C. Gillies, D.A. Waring, NASA  $\mu$ g Materials Science Conf. Huntsville, 10-11 June 1996, NASA conf. Publi. 3342, 345-350.
- [11] K. Kinoshita, H. Kato, S. Yoda, Xth European Symp. Physical Sciences in Microgravity, St Petersburg, 15-20 June 1997.
- [12] N. Duhanian, T. Duffar, C. Marin, J. Abadie, M. Chaudet, E. Dieguez Xth European Symp. Physical Sciences in Microgravity, St Petersburg, 15-20 June 1997.

Advanced Gradient Heating Facility (AGHF)

## Directional Solidification of Al - 1.5 wt.% Ni Alloys

Principal Investigator:

Dr. Henri Nguyen Thi  
Université d'Aix-Marseille III  
Marseille, France

# **DIRECTIONAL SOLIDIFICATION OF Al - 1.5 wt% Ni ALLOYS DURING THE LMS - AGHF - ESA7 EXPERIMENTS**

**H. Nguyen Thi, B. Billia, Y. Dabo**

Laboratoire MATOP, Associé au CNRS, Université d'Aix-Marseille III

Faculté des Sciences St-Jérôme, Case 151,

13397 Marseille Cedex 20, France

and

**D. Camel, B. Drevet, M.D. Dupouy, J.J. Favier**

DTA/CEREM/DEM/SE. CENG. 17 Rue des Martvrs.

---

38054 Grenoble Cedex 9, France

## **(1) OBJECTIVES**

The final properties of alloys depend strongly on the microstructures formed at the solid - liquid interface during the solidification process. Thus, a precise understanding of this pattern formation is essential to produce high quality materials. In ground-based experiments, even when solidification is performed in a both thermal and solutal stabilizing configuration, strong convective flows remain present due to residual radial thermal gradients. The purpose of the LMS - AGHF - ESA7 experiment is to examine cellular and dendritic arrays under conditions in which convection is minimized and diffusive phenomena are dominant. From these experimental results, scientists will better understand the dynamics of the microstructures and also enlighten the influence of convection on the solidification.

## **(2) BACKGROUND**

During the directional solidification of a binary alloy, three experimental parameters control the morphology of the solid - liquid interface, namely the initial solute concentration, the temperature gradient at the solid - liquid interface and the growth rate. If the first two factors are maintain constant, at slow growth velocities, the solidification front is planar; as the rate is increased, above a critical value, the interface forms a cellular microstructure which becomes dendritic at higher growth velocities. This pattern formation is associated to the Mullins - Sekerka instability [1] and much effort has been devoted to predict the characteristics of the cell or dendritic arrays as a function of the solidification control parameters [2].

However, convection in the melt is well known to be the source of various perturbative effects which can modify or mask some important physical mechanisms [3]. Attempts are often made in directional studies to eliminate buoyancy convective motion in the liquid phase. A simple way of doing this is to ensure that the density gradient is everywhere vertical, the heaviest material being at the bottom. This occurs when growth takes place upwards in an alloy system in which the rejected solute is denser than the solvent. Nevertheless, even in this experimental configuration, it is well known that strong convective flow can exist owing to radial effects, especially in the cellular growth regime [4-6].

As shown in previous experiments [7, 8], a comparative study between samples solidified at 1g and under microgravity is worth to provide critical information concerning the influence of convection upon the directional solidification. Al - 1.5 wt% Ni is well adapted for such a study as the distribution coefficient is much lower than one (i.e. the solute is almost completely rejected at the front during the solidification process) and the solute (nickel) is denser than the solvent (aluminum).

### **(3) EXPERIMENT**

#### **LMS - AGHF - ESA7 experiments**

During the LMS mission in June 1996, two Al - 1.5 wt% Ni alloys were solidified in the Advanced Gradient Heating Facility (AGHF) of ESA which is a Bridgman type furnace. After being machined into rods of 8 mm in diameter and 218 mm in length, the samples were elaborated in a boron nitride crucible. To measure temperature gradient and solidification rate during the whole experiment, the cartridges were equipped with 12 thermocouples, glued on the outer surface of the crucible. The processing parameters were predetermined by experiments performed in the breadboard and engineering models of the AGHF in the Centre National d'Etudes Spatiales (CNES) in Toulouse (France).

For both experiments, the thermal gradient was about  $(35 \pm 2)$  K/cm but two different pulling rate profiles were used. In one experiment, a single low solidification velocity was imposed ( $V = 0.05$  mm/min) whereas in the second run, two growth rates were successively applied ( $V = 0.2$  mm/min and  $0.1$  mm/min). After a solidified length of typically three centimeters, the residual liquid was quenched by a rapid furnace displacement ( $V = 10$  mm/min). This stopped the solidification and froze the interface microstructure.

#### **Determination of longitudinal concentration profile**

The axial concentration profiles are obtained by analyzing in grey levels the X - Ray picture of each sample. This technique presents the great advantage to be non destructive and also enable us to precisely determine the successive steps of the experiment, namely the initial position of the interface and final position of the solidification front just before the quench. The solute concentration is then given in arbitrary unit and will be calibrated with chemical or microprobe analysis in future.

## Metallographic procedure

Since metallic alloys are opaque, a somewhat tedious procedure has to be used to obtain the morphology of the solid - liquid interface. During the solidification, after stationary conditions are reached, the shape of the solidification front is fixed by quenching the residual liquid phase. After the experiment, the morphology of the solidification front is revealed by polishing on a longitudinal section of the sample, containing the quenched interface. Transverse sections of the samples are also obtained by the same metallographic procedure.

## (4) RESULTS

### Concentration profiles

The solute distribution in a directionally solidified alloy depends strongly on the type of transport in the liquid phase [9]. In  $\mu\text{g}$  experiments, the absence of convection leads to a diffusive mass transport in the melt as opposed to 1g-experiments where convecto-diffusive transport is dominant. Nevertheless, for the considered convection, namely upwards solidification with a solutal stabilizing effect, a weak longitudinal macrosegregation is expected with a large radial macrosegregation [6]. This point is confirmed by the concentration measurements on 1g-samples as shown in Fig.1. After an initial transient, the average solute composition is quite constant at a value slightly lower than the nominal value. This clearly shows that the convective roll formed weakly mixes with the bulk liquid.

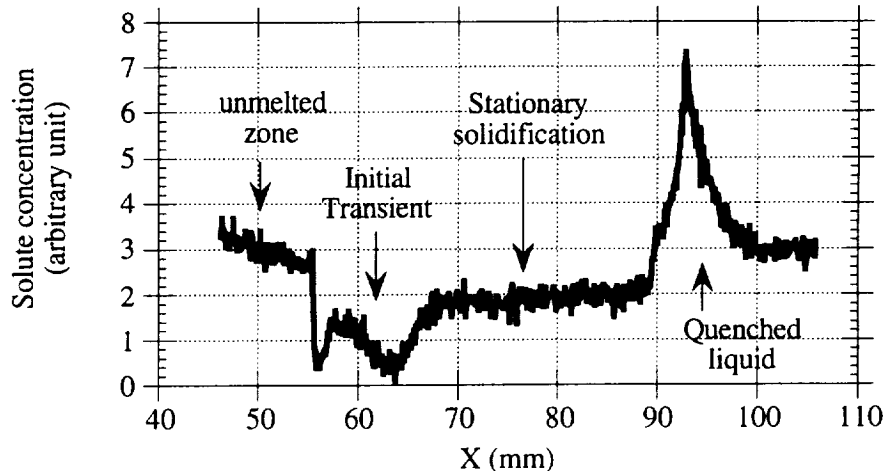


*Figure 1: Longitudinal segregation in Al - 1.5 wt % Ni sample  
solidified at 1g ( $G = 33 \text{ K/cm}$  and  $V = 0.06 \text{ mm/min}$ )*

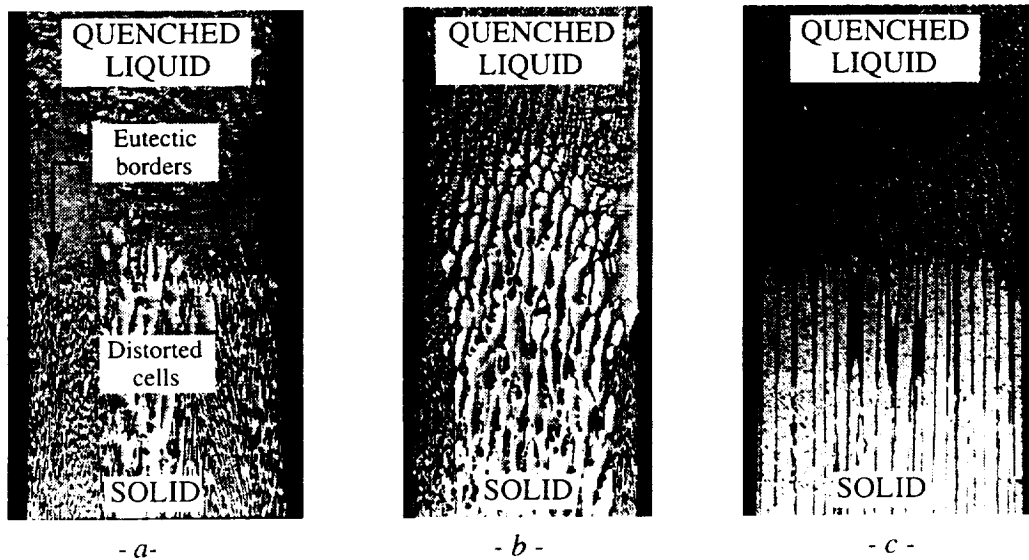
### Macroscopic shapes of the solidification front

Fig.2 shows typical solidification fronts for sample elaborated at 1g (Fig.2a and 2b) and in  $\mu\text{g}$  (Fig.2c). The effect of convection results in a severe distortion of the solidification front which could be divided in a cellular region and eutectic borders. The microstructure is obviously not

uniform across the specimen cross section and therefore a large radial macrosegregation is expected.

The explanation for this effect is that fluid flow occurs as a consequence of gravity. The flow is as described in [4, 6]: the interdendritic liquid which is solute richer, therefore denser than the bulk liquid, moves towards any depressed region of the solidification front and further retards solidification there. When the local solute concentration reaches the eutectic composition, eutectic growth occurs and the lighter liquid moves upwards away from the solidification front. Therefore, if the interface is not completely horizontal, convection inevitably occurs.

In real experimental conditions, this may happen because of the differences in thermal conductivities of the solid, the liquid and the crucible material. This may also be produced by microconvection in the tip zone [4]: when one cell in the cellular array lags behind its neighbors, the denser liquid flows down, further eliminating other neighboring cells and producing the distorted solid - liquid interface.



*Figure 2: Longitudinal sections of Al - 1.5 wt% Ni samples solidified :  
 at 1g: - a -  $V = 0.060$  mm/min,  $G = 33$  K/cm and - b -  $V = 0.107$  mm/min,  $G = 37$  K/cm  
 in  $\mu$ g: - c -  $V = 0.053$  mm/min,  $G = 34$  K/cm*

### Microstructures of the solid - liquid interface

Typical cross sections, four millimeters under the quenched interface, are presented in Figure 3. In 1g-specimen (Fig.3a), the microstructure is not uniform across the sample section: in the core of the sample, the microstructure is cellular but becomes more and more dendritic close to the eutectic border. A strong tendency for these dendrites to grow towards the eutectic region is also observed. Moreover, the location where these eutectic regions take birth is not correlated with the symmetry of the thermal conditions applied by the furnace to the sample. As for the AGHF samples grown at 1g, this feature is always obtained and, in most of experiments carried out in our laboratory, the solidification front could be described as consisting of two parts: a cellular or dendritic array and an eutectic zone (Fig.3b). In that case, the cells are said "clustered". On the

contrary, in  $\mu\text{g}$ -sample (Fig.3c), the cellular array is rather uniform and covers the whole section.

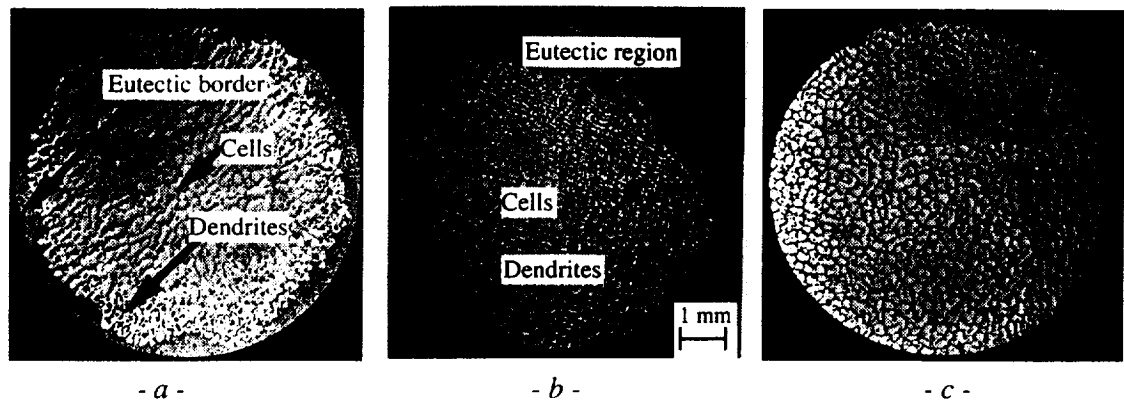


**Figure 3:** Transverse sections of Al - 1.5 wt% Ni samples solidified :  
 at  $1\mu\text{g}$ : - b -  $V = 0.06 \text{ mm/min}$ ,  $G = 33 \text{ K/cm}$  and - c -  $V = 0.20 \text{ mm/min}$ ,  $G = 24 \text{ K/cm}$   
 in  $\mu\text{g}$ : - a -  $V = 0.23 \text{ mm/min}$ ,  $G = 33 \text{ K/cm}$

These conclusions remain valid for experiments carried out at the Laboratory, in the same range of solidification rates. For a higher value of the growth rate, the solid - liquid interface becomes obviously dendritic but the macroscopic distortion of the front does not occur (Fig.4). The influence of the convection is thus more important in the range of low velocities, for cellular or weakly dendritic growth.

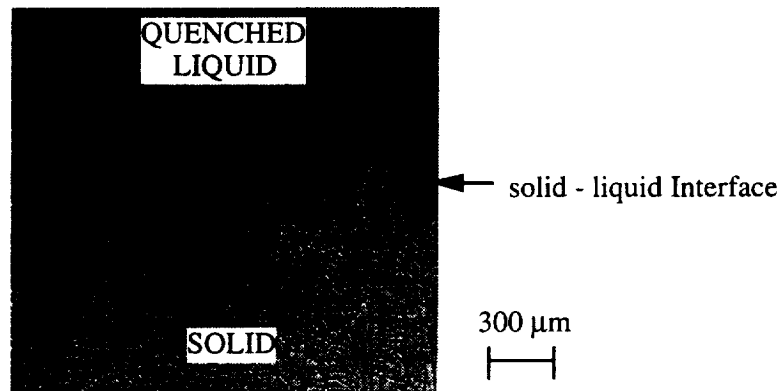


**Figure 4:** Longitudinal section of Al - 1.5 wt% Ni samples solidified at  $1\text{g}$ :  $V = 1.7 \text{ mm/min}$ ,  $G = 24 \text{ K/cm}$

All these results are in very good agreement with the model of Dupouy et al, for dendritic growth [6]. Assuming that convection will have a significant effect on the solidification as soon as the ratio  $\Gamma$  of the characteristic velocity of the convective flow  $U^*$  to the solidification rate  $V$  is greater than unity, it is possible to draw the theoretical curve of the transition between the convective and the purely diffusive regimes (Fig.5). Experimental data are also reported in this figure. Circles symbols correspond to cellular microstructures which are strongly perturbed by convection and square symbol to one experiment where the solidification front is dendritic but with no visible influence of the convection.

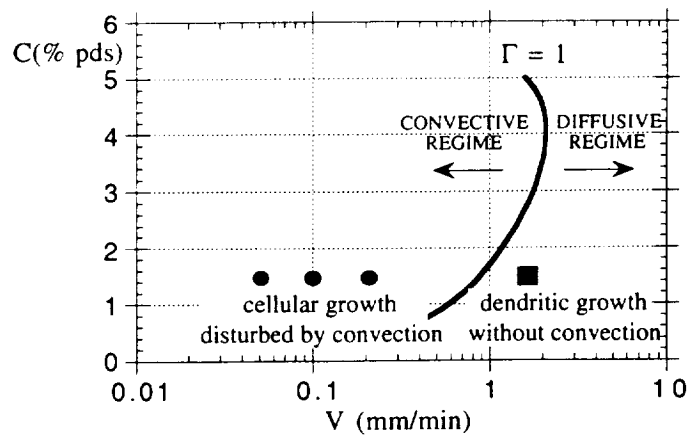


*Figure 5: Transition curve between convective and diffusive regimes for Al - Ni alloy in the composition - growth rate diagram*

## (5) CONCLUSIONS

This comparative experimental study has shown that the coupling between the natural convection and the morphological microstructures can be strong even when solidification is performed in a both thermal and solutal stabilizing configuration. In that case, ground based experiments are invariably perturbed by the thermosolutal convection and, consequently are totally unsuitable for a study of cellular or dendritic arrays. For this alloy, only  $\mu g$  environment with a dominant diffusive transport can provide reliable data.

## (6) ARTICLES/PRESENTATIONS RESULTING FROM THE FLIGHT

- 1) Proceeding of the « *Joint Xth European and VIth Russian Symposium on Physical Sciences in Microgravity* », St-Petersburg (Russia), 15-21 June 1997
- 2) Proceeding of the « *Sèmes Journées Européennes de la Thermodynamique Contemporaine* », Toulouse (France), 16-19 September 1997

## (7) ACKNOWLEDGMENTS

The authors are greatly indebted to the European Space Agency and specially to J. Stroede. The financial and technical support of the Centre National d'Etudes Spatiales is also gratefully acknowledged.

## **(8) REFERENCES**

- [1] W.W. Mullins and R.F. Sekerka, *J. Appl. Phys.* 35 (1964) 444
- [2] J.S. Langer in *Chance and Matter, Lectures on the Theory of Pattern Formation, Les Houches Summer School* (Eds by J. Souletie, J. Vannimenus and R. Stora, North Holland (1986), 689)
- [3] M.E. Glicksman, S.R. Coriell and G.B. McFadden, *Ann. Rev. Fluid Mech.* 18 (1986) 307
- [4] M.H. Burden, D.J. Hebditch and J.D. Hunt, *J. of Cryst. Growth* 20 (1973) 121
- [5] J.D. Verhoeven, J.T. Mason and R. Trivedi, *Metall. Trans. A* 17A (1986) 991
- [6] M.D. Dupouy, D. Camel and J.J. Favier, *Acta Metall.* Vol.37, N°4 (1989) 1143
- [7] D. Camel, J.J. Favier, M.D. Dupouy and R. Le Maguet, *Proceedings of Vith European Symposium on Material Sciences under Microgravity, ESA - SP 256* (1987) 317
- [8] B. Drevet, D. Camel, C. Malmejac, J.J. Favier and H. Nguyen Thi, Q. Li, B. Billia, *Adv. Space Res.* Vol.16, n°7 (1995) 173
- [9] J.P. Garandet, J.J. Favier and D. Camel, *Handbook of Crystal Growth, Vol.2B* (1994) 659

## **SUMMARY OF THE LMS - AGHF - ESA7 EXPERIMENT**

The final properties of alloys depend strongly on the microstructures (cells and dendrites) formed at the solid - liquid interface during the solidification process. Thus, a precise understanding of this pattern formation is essential to produce high quality materials. In ground-based experiments, even when solidification is performed in a both thermal and solutal stabilizing configuration, strong convective flows remain present due to residual radial thermal gradients. The purpose of the LMS - AGHF - ESA7 experiment is to examine cellular and dendritic arrays under conditions in which convection is minimized and diffusive phenomena are dominant. In addition, a comparative study between samples solidified at 1g and under microgravity is worth to provide critical information concerning the influence of convection upon the directional solidification. From these experimental results, scientists will better understand the dynamics of the microstructures and also enlighten the influence of convection on the solidification.



Advanced Gradient Heating Facility (AGHF)

## Interactive Response of Advancing Phase Boundaries to Particles

Principal Investigator:

Dr. Ulrike Hecht  
ACCESS  
Aachen, Germany

# INTERACTIVE RESPONSE OF ADVANCING PHASE BOUNDARIES TO PARTICLES

U. Hecht and S. Rex, ACCESS e.V., Intzestr. 5, D-52072 Aachen, Germany

MISSION: LIFE AND MATERIALS SCIENCE - LMS / JUNE 1996  
EXPERIMENT: INTRAPP (ESA5)  
FACILITY: ADVANCED GRADIENT HEATING FACILITY (AGHF)  
DOCUMENT: PROGRESS REPORT / JUNE 1997

## 1. INTRODUCTION

The high strength/density ratio makes particle reinforced aluminum alloys with precipitation-hardenable matrices e.g. 2XXX attractive for use in aircraft and automobile structural parts. The most effective way to achieve high quality - low cost PRMMC products is via casting process. Development and application

1. particle pushing at coarsening grains in the mushy zone of the fusion interface during stabilization
2. particle pushing and the transition from pushing to engulfment in directional solidification with planar interface within the initial transient

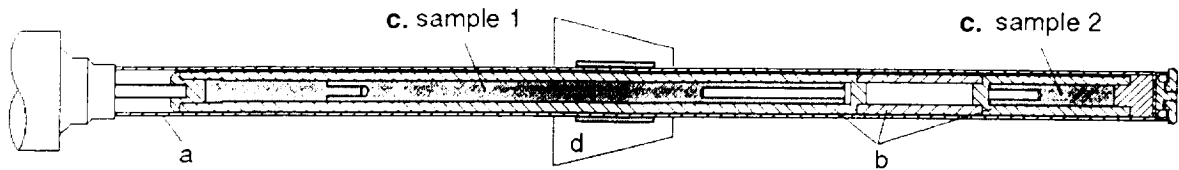


**Figure 1.** Cartridge design

**a.** cartridge tube (Ta-W 2.5 wt%), **b.** crucibles and isolating ring (BN-ZrO<sub>2</sub> composite), **c.** samples (2014 + 10 vol% Al<sub>2</sub>O<sub>3</sub>), Ø 8 \*206 mm and Ø 8 \*39 mm **d.** liquid metal ring  
A number of 14 Inconel-sheathed thermocouples (typ N Ø 0.5) were placed in individual grooves at the outer circumference of the crucibles at different longitudinal position.

## 2.1. Sample material

The sample material consisted of the commercial composite 2014 + 10 vol% Al<sub>2</sub>O<sub>3</sub> (DURALCAN), the particles being of nominally 13 µm mean size and of angular morphology with an elongation factor close to unity. Figure 2 shows the solidification characteristics (2a.) and the microstructure (2.b) of the sample material in the as extruded condition. Table 1. contains the standard composition of the matrix alloy.

For the investigation of particle / interface interactions in this composite, knowledge about the segregation behavior of the matrix, as well as a reasonable estimation of the magnitude of repulsive forces is required. Qualitatively, the segregation behavior and the invariant reactions in 2014 correspond to the quaternary system (Al-Cu-Mn-Si) as assessed by Mondolfo [1]. The magnitude of repulsive forces is related to interfacial energies in the three phase system: particle / liquid / solid, or else to constants of molecular interaction like the Hamaker constant [2] or the London-van der Waals constant [3]. For Al<sub>2</sub>O<sub>3</sub> in 2014 the interfacial energies  $\sigma_{ps}$ ,  $\sigma_{pl}$  and  $\sigma_{sl}$  are taken from literature data referring to aluminum or aluminum alloys [4,5]. The interfacial energy difference, calculated according to [6], gives  $\Delta\sigma = 0,68$  [N/m], the accuracy being estimated to  $\pm 0,2$  [N/m].

## 2.2. Processing parameters

The parameters, heater temperature and furnace velocity, were defined such as to obtain directional melting of the two samples, followed by directional solidification of sample 1 at two different

furnace velocities and subsequent solidification of sample 2 at a constant cooling rate of 4 [K/min], the furnace being immobile.

For sample 1 the parameters were selected as to obtain an interface position (isotherm 620°C) close to the middle of the adiabatic zone and moreover, to obtain the transition from particle pushing to engulfment prior to the morphological destabilization of the planar interface.

Figure 3 summarizes the processing parameters applied in the two µg- and the corresponding 1g-reference runs. Figure 4 shows typical gradient profiles along the directionally solidified sample 1.

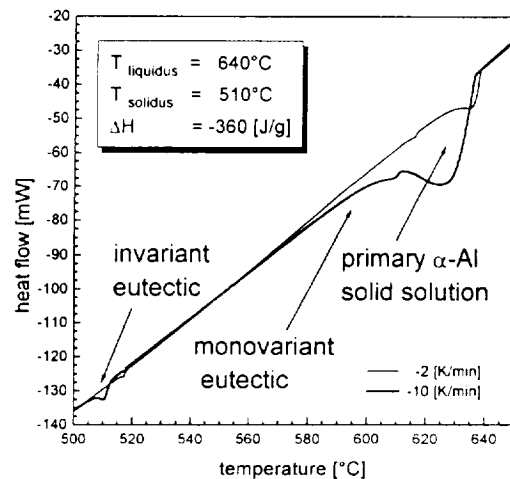


**Figure 2a.**

Solidification characteristics of the matrix alloy determined by differential scanning calorimetry (typ Perkin-Elmer DSC 7)

**Table 1.** Chemical composition of the matrix alloy 2014

Element [wt%]	Cu	Si	Mn	Mg	Fe	Cr	Ti	Zr	Al
min.	3.90	0.50	0.40	0.40	-	-	-	-	bal.
max.	5.00	1.20	1.20	0.80	0.10	0.15	0.15	0.25	bal.



**Figure 2 b.** Microstructure in the as extruded condition. The alignment of the alumina particles along the direction of extrusion (vertical) can be observed.

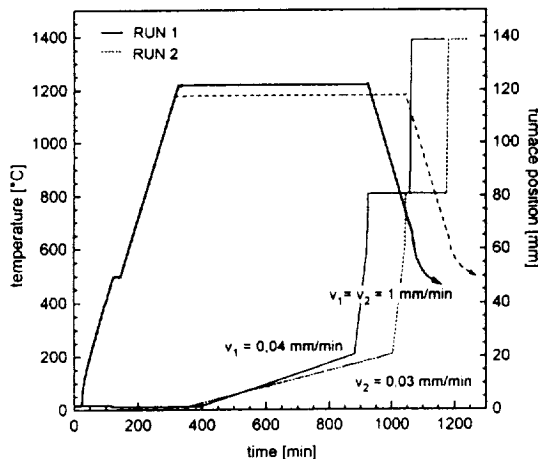


**Figure 3.** Processing parameters Diffuser temperature and furnace velocity profiles applied during run 1 (FM1, GM1) and run 2 (FM2, GM2). The two "quenching" operations were meant for rapid furnace positioning, rather than for structural conservation of the interface.

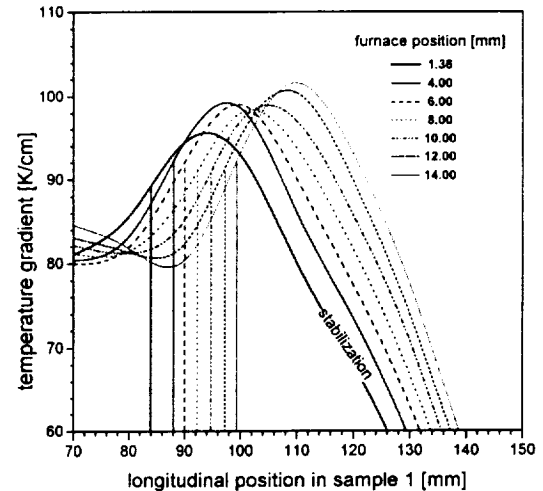


**Figure 4.** Gradient profiles Axial profiles of the thermal gradient for consecutive furnace positions in FM2 and the corresponding positions of the interface ( $v = 0.03$  mm/min)

### 2.3. Evaluation techniques

The evaluation is based on the analysis of the particle distribution and its correlation with the thermosolutal conditions during solidification. For this purpose the samples were cut along their longitudinal axis by using a diamond wire saw of 170  $\mu\text{m}$  wire diameter, one sample half being dedicated to longitudinal analysis, the second to the preparation of transversal metallographic sections.

The analytical techniques that have been employed are: microscopy (LM and SEM), interactive automated image analysis and EDX / WDX for measurement of solutal profiles in line scans and area mappings. The thermal history is based on as-registered thermocouple data, while ongoing work is dedicated to a more detailed simulation of the thermal field.



In addition, stage mapping of the elements Cu, Mn, Mg and O was performed for the samples FM2 and GM2 in order to check if the longitudinal scans are indeed representative. Figure 7 shows one longitudinal scan through the mapping area in FM 2 in comparison to the lateral scatter. From the line scans the critical concentration of the individual alloying elements was extracted as corresponding to the respective position of beginning engulfment. Figure 8 and figure 9 show the evolution of two representative alloying elements, copper and manganese, along the initial transient of the flight and ground reference samples respectively.

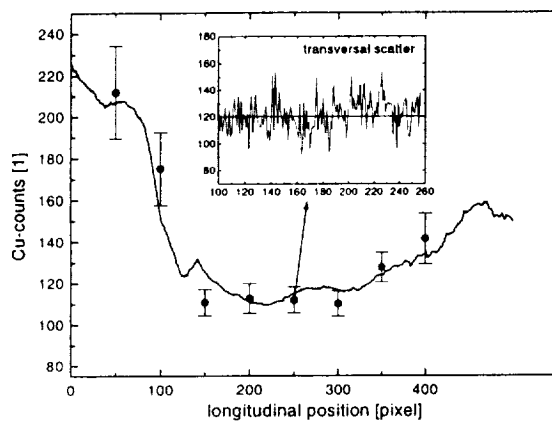


**Figure 7.** Sections through the area mapping of the copper concentration in FM2. Area size: 5 \*10mm  
The error bars indicated at selected positions of the longitudinal scan represent the transversal scatter.

In order to define the "critical concentration", the multiply alloyed matrix is reduced to an equivalent binary matrix via the transformations [10,11]:

$$(2) \quad \begin{aligned} c_e &= \sum c_i, & \text{for } i = 1 \text{ to } 5 \\ m_{i,e} &= (\sum c_i \cdot m_{i,i}) / c_e \\ k_e &= (\sum c_i \cdot m_{i,i} \cdot k_i) / c_e \cdot m_{i,e} \end{aligned}$$

Here, the indices "i" are related to the individual binary systems between Al and the alloying elements, while "e" represent the equivalent binary data.

These transformations are rather simple. A more refined analysis of the segregation behavior based on thermodynamics of the multiply alloyed matrix will further enhance the evaluation.

This is especially true with respect to the partition coefficients and the liquidus slopes. In ternary or higher alloyed systems the sign of the liquidus slope changes for certain elements (e.g. Mn in Al-Cu-Si-Mn) from negative to positive, as the system passes into the binary eutectic region, although the partition coefficient remains subunitary. It depends on the sign of  $m_i$ , whether the solutal distortion induced by a particle leads concave or convex deformation of the interface.

A check of the matrix segregation has been made by solidifying the particle free alloy 2014 at constant cooling rate and measuring the solute profile across a dendrite arm via EDX. The segregation pattern, represented in figure 10, shows a change from increasing ( $m_{iMn} < 0$ ) to decreasing Mn-concentration ( $m_{iMn} > 0$ ) related to intermetallic phase nucleation in the system Al-Cu-Mn-Si-Mg [1].

A detailed investigation of the segregation profiles obtained during directional solidification of the INTRAPP-samples will address this behavior of Mn, which is representative for specific elements in higher alloyed systems.

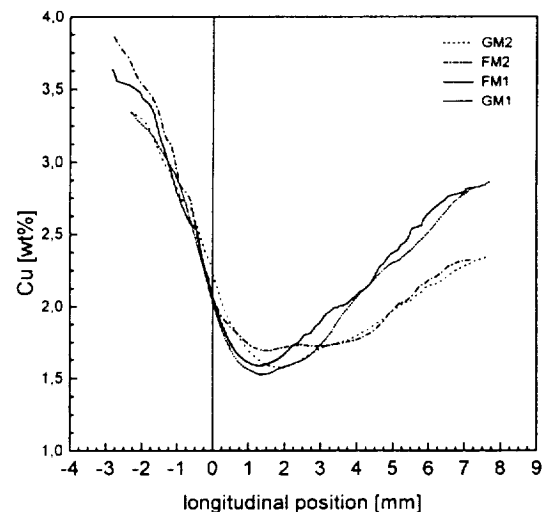


**Figure 8.** Axial concentration profiles for the main alloying element Cu.

The sample position "0" corresponds to the initial position of the liquidus temperature + 10°C, being the position at which the string-like particle agglomerates, originating from coarsening grains in the mushy zone, cease to exist.

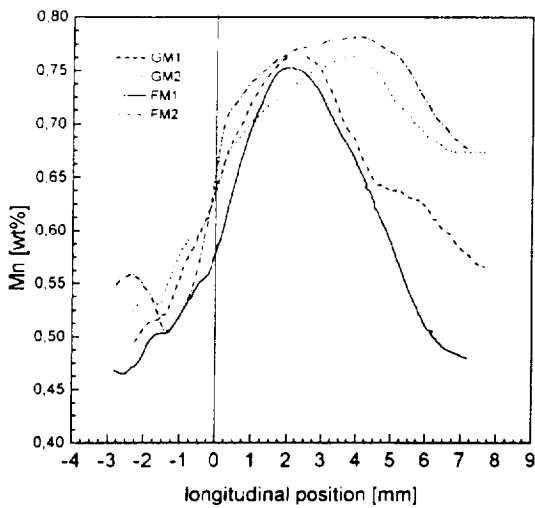


**Figure 9.** Axial concentration profiles for the alloying element Mn. The position "0" corresponds to the initial position of the liquidus temperature + 10°C, e.g. to the position at which the string-like particle agglomerates, originating from coarsening grains in the mushy zone, cease to exist.

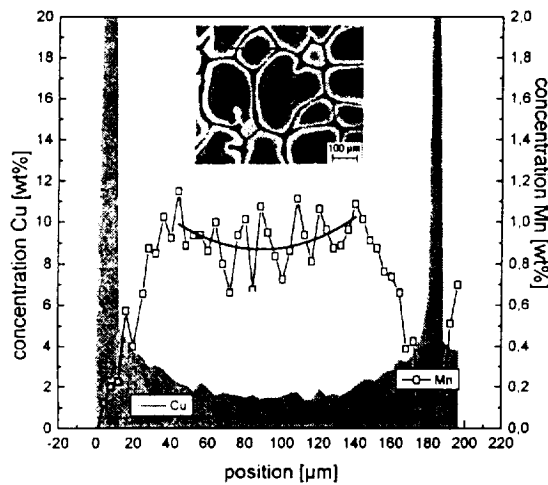


**Figure 10.** Solute profile across a globulitic dendrite obtained during unconstrained solidification of the particle-free matrix alloy 2014 at 2 [K/min]. Colour etching with Weck's reagent gives an optically accessible view of the segregation. The EDX scan line is indicated in the inserted image.

To date, the critical conditions for the transition from particle pushing to engulfment should be regarded as an order of magnitude analysis only. They are summarized in Table 2.

Here, the effective melt viscosity is calculated according to:

$$(3) \eta = \eta_0 \cdot (1 + 2.5 f_p + 10.05 f_p^2) \quad [8]$$

$$(4) f_p = (\pi R^2 z) \cdot f_{p0} / (\pi R^2 z'),$$

where  $z$  represents the pushing length,  $z'$  the width of a boundary layer where the pushed particles accumulate e.g.  $z'=1.2$  [mm],  $R$  the sample radius, and  $f_{p0}$  the initial volume fraction of particles in the MMC.

Based on these data, the critical velocity is calculated according to Pötschke and Rogge [7] and included in table 2. It results that the experimental data are in good agreement with the model predictions, especially when taking into account that the interface velocity is lower than the furnace translation velocity. This correction will be included during further work. An analysis of errors associated with the critical velocity values will be addressed together with a more rigorous treatment of the segregation in the matrix.

Beside the transition from pushing to engulfment, a quite challenging question arises with respect to the evolution of the pushing configurations along the initial transient. We expect these configurations to be subcritical force equilibria, continuously adjusting to the change of governing variables ( $c$ ,  $\eta$ ,  $v$ ,  $G$ ). The adjustment process is realized through changes of the local curvature and of the liquid gap width. Subcritical force equilibria are consistent with the concept of the critical velocity, or more general of the "critical conditions", as being the maximum velocity - or the maximum concentration etc. - for which force equilibrium can be established.

Transferring the model of Pötschke and Rogge to transient pushing along the initial transient predicts, that with increasing concentration of the alloying element both forces increase, with the viscous drag force increasing more rapidly than the molecular repulsive force. Consequently, force equilibrium is established at gradually decreasing width of the liquid gap. Figure 11 principally shows the evolution of subcritical force equilibria with changing curvature of the interface according to [7]. The analysis of the experimental data on transient pushing is in progress.

**Table 2.** Critical conditions for the transition from particle pushing to engulfment

Run	G [K/cm]	c [wt%]	$ m_1 $ [K/%]	k	$\eta$ [Ns/m <sup>2</sup> ]	vexp. [μm/s]	vcrit. [7] [μm/s]
Flight 1	109	2.93	3.20	0.2	3.9E10 <sup>-3</sup>	0.66	0.60
Flight 2	87	3.04	2.98	0.2	6.3E10 <sup>-3</sup>	0.50	0.43
Reference 1	101	2.74	3.10	0.2	3.9E10 <sup>-3</sup>	0.66	0.61
Reference 2	88	2.98	3.03	0.2	6.3E10 <sup>-3</sup>	0.50	0.44

Data for calculation of the critical velocity in 2014 / Al<sub>2</sub>O<sub>3</sub> are summarized in [12]

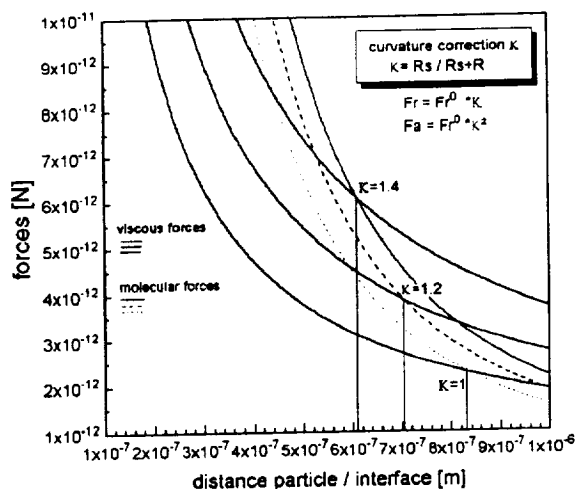


**Figure 11.** Subcritical force equilibria configurations calculated according to [7] for a 20 μm-sized Al<sub>2</sub>O<sub>3</sub> particle in the equivalent binary matrix Al-X, as function of the particle induced interface curvature (e.g. concentration).

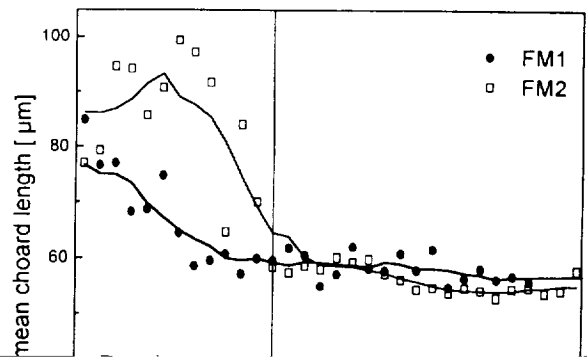
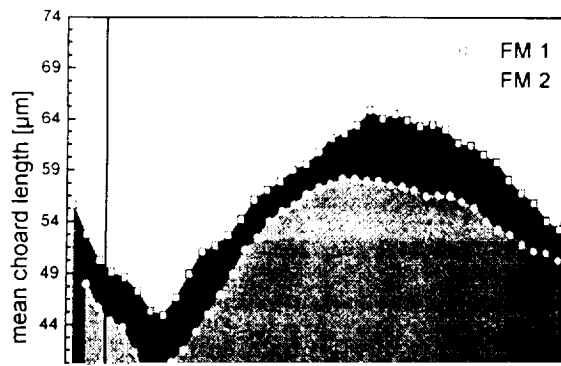
### 3.2 Particles at dendritic solid/liquid interface in constrained and unconstrained growth

The INTRAPP samples contain two regions with dendritic morphology: In samples 1 constrained dendritic growth was generated over a length of 40 mm, at  $v=1.0$  [mm/min] and a thermal gradient of 85 to 105 [K/cm]. The samples 2 were designated to unconstrained dendritic growth at constant cooling rate, but due to residual axial temperature gradients the dendritic structure is columnar with a transition to equiaxed growth in the region of the cartridge hot end only. In the dendritic regions particle distributions were measured by interactive automated

image analysis on longitudinal sections of the flight samples.

Among several distribution features, the mean choard length (MCL) has been selected for evaluation. The MCL is measured perpendicular to the sample axis, thus representing a means to quantify the spacing between stringlike particle agglomerates that occur in columnar dendritic structures. Figures 12 and 13 show the evolution of the MCL in the flight samples, for solidification at a furnace velocity of 1 mm/min and at constant cooling rate of 4 [K/min], respectively. The evolution of MCL with proceeding solidification gives interesting insight into the dynamics of particle distribution in relation to spacing selection during transients that are induced by velocity changes etc.. Its absolute value scarcely bears information on the mechanism of particle incorporation. More details can be visualized in LM with an appropriate etching technique (figure 14) or by SEM (figure 15). They show that the particles are located inbetween dendrite arms e.g. in eutectic surroundings, for both, ground and flight samples.

Models based on steady state pushing, although validated for planar interface [7], fail to explain the observed interdendritic particle distribution e.g. the critical velocity for unconstrained growth configuration calculated according to [7] ranges from 10<sup>-13</sup> to 10<sup>-14</sup> [m/s] depending on the concentration. This extreme reduction of the critical velocity compared to the constrained planar growth is due to the fact, that a particle of lower thermal conductivity than the melt depresses the interface via both, thermal and solutal distortion. This order of magnitude analysis suggests, that interdendritic particle incorporation is based on entrapment mechanisms, rather than on "pushing in force equilibrium".





## REFERENCES

1. L.F. Mondolfo: Aluminum Alloys. Structure and Properties, Butterworth and Co. Publishers Ltd., London, 1976, pp. 656
2. H.C. Hamaker: Physica IV. No 10, 1937, pp. 1058-1072
3. D.E. Temkin et al.: Sov. Phys. Crystallogr., 1977, vol. 22, pp. 13-17
4. L.E. Murr: Interfacial Phenomena in Metals and Alloys, Addison Wesley Publishing Co., Reading, MA, 1975, pp. 101-131
5. J.G. Li: Ceramics Int., 1994, vol. 20, pp. 391-412
6. G. Kaptay: Mat. Scie. Forum, 1996, vol. 215-216, pp. 467-474
7. J. Pötschke and V. Rogge: J. Cryst. Growth, 1989, vol. 94, pp. 726-738
8. S.R. Coriell et al.: J. Cryst. Growth, 1994, vol. 140, pp. 139-147
9. D.M. Stefanescu and F. Rana: in Metallurgical Development and Control in Materials Processing, D.R. Durham and A. Saigal, eds., 1989, vol. 14, pp. 95-100
10. M. Bobadilla et al.: J. Cryst. Growth, 1988, vol. 89, pp. 531-544
11. M. Rappaz et al.: Metall. Trans A, 1990, vol. 21A, pp. 1767-1782
12. U. Hecht and S. Rex: Met. Trans., 1997, vol. 28 A, , pp. 867-874

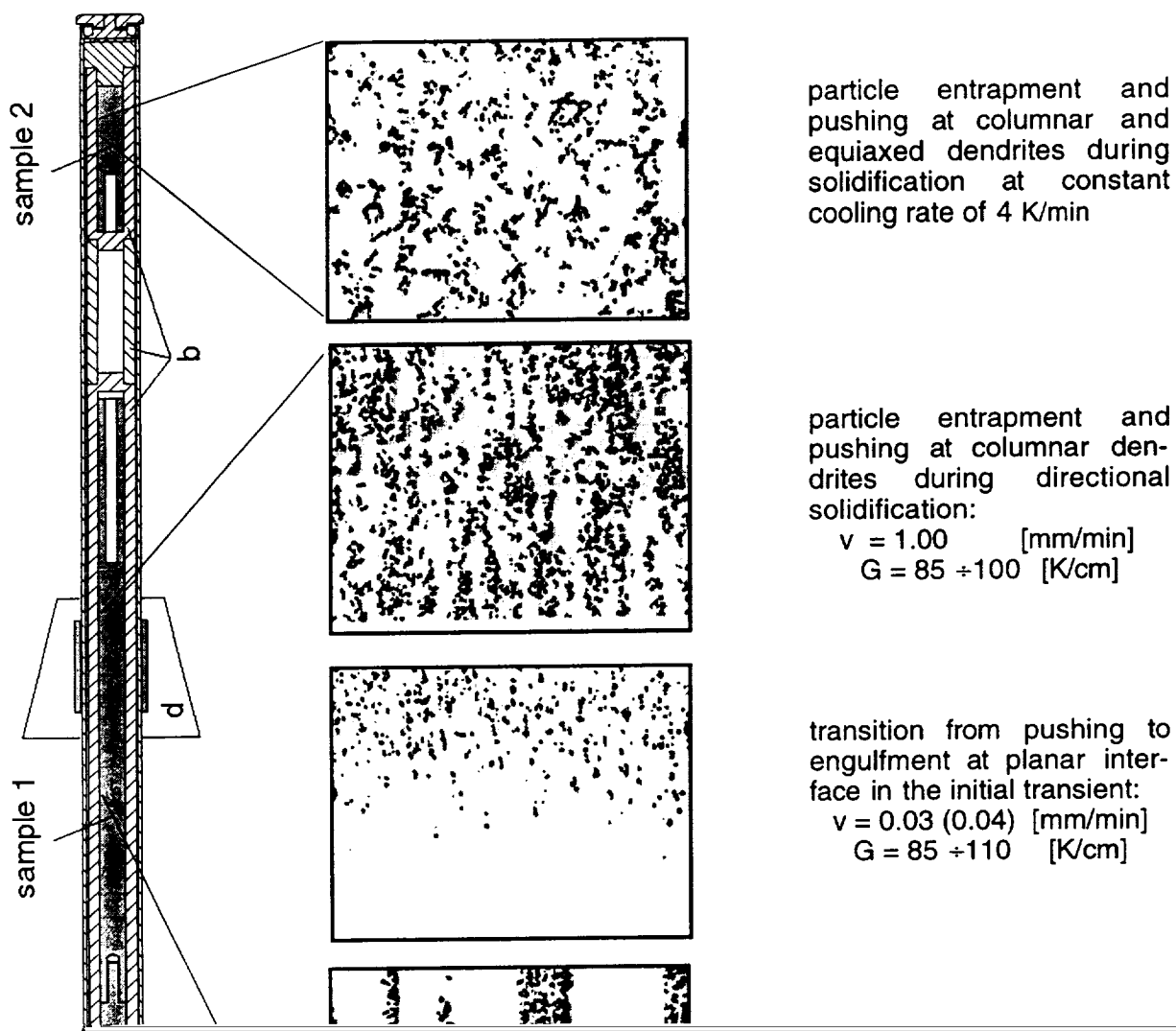
## List of symbols

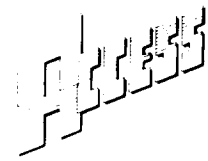
$\eta$	effective viscosity of the melt	Ns/m <sup>2</sup>
$\eta_0$	viscosity of the pure melt	Ns/m <sup>2</sup>
$f_p$	effective volume fraction of particles	
$f_{p0}$	initial volume fraction of particles	
$v$	interface velocity (furnace velocity)	m/s
$c$	concentration of alloying elements	wt%
$G$	temperature gradient	K/m
$\Delta\sigma$	interfacial energy difference	N/m
$R$	particle radius	m
$a_0$	atomic distance in the melt	m
$\mu$	ratio of thermal conductivity particle /melt	
$ m_l $	slope of the liquidus line	K/wt%
$k$	equilibrium partition coefficient	
$D$	diffusion coefficient	m <sup>2</sup> /s

## Acknowledgment

This work was financially supported by the German Agency for Space Affairs DARA GmbH under grant FKZ 50WM9565.

## OVERVIEW OF RESULTS





## INTERACTIVE RESPONSE OF ADVANCING PHASE BOUNDARIES TO PARTICLES INTRAPP

U. Hecht and S. Rex, ACCESS e.V., Intzestr. 5, D-52072 Aachen, Germany

Many natural and artificial composite materials offer unique properties that cannot be obtained with a single material. Small ceramic particles for instance, when mixed into aluminum alloy, lead to an increase of the overall strength and abrasive resistance, making the material attractive for use in aircraft and automobile components. It is well known, that the properties of the composite material do not only result from the rule of mixture, but that they are highly sensitive to newly created characteristics of the material. Such characteristics are the structure of the interface between particles and the base alloy and the distribution of particles inside the base alloy. It is also known that particles are preferentially located in specific regions of the base alloy, for instance inbetween the tiny tree-like structures called dendrites, that grow from the molten alloy during solidification. Here, the particles form net-like agglomerates and can later on act as crack-paths. A reason for this behavior might be the very small forces, some  $10^{-8}$  [N] small, that act between the growing solid and the ceramic particle, pushing the particle further into the liquid as growth proceeds. The forces originate from fluctuations of the electric charge inside the atoms, much like the forces that hold liquid atoms together in the condensed state.

The microgravity experiment INTRAPP, performed in the Advanced Gradient Heating Facility (AGHF) during the Spacelab Mission-LMS in June '96, investigated the behavior of alumina particles (mean size 13  $\mu\text{m}$ ) in interaction with advancing solid / liquid interfaces. The samples consisted of the aluminum based commercial composite material 2014 + 10 vol%  $\text{Al}_2\text{O}_3$ . The microgravity results show a large variety of particle behavior: at plane solidification front particles were pushed over several mm like being swept away by a snowplough, before getting engulfed into the solid. At non-planar front, particles were found to be located inbetween the dendrite arms. Moreover, the large solidification interval of the alloy allowed to show particles being pushed at coarsening grains in the mushy zone.

From the manifold data, particle pushing at plane front was evaluated first and shows good agreement with the theoretical model of Pötschke and Rogge. It also shows the complexity of transferring theoretical models to real commercial materials. This becomes more evident when processing conditions come closer to application, e.g. when dendritic growth is generated in the base alloy: For these situations further modeling activities are necessary when more than a qualitative prediction of the particle distribution is desired. The



Advanced Gradient Heating Facility (AGHF)

## Particle Engulfment and Pushing by Solidifying Interfaces

Principal Investigator:

Dr. Doru Stefanescu  
University of Alabama  
Tuscaloosa, Alabama

# Particle Engulfment and Pushing by Solidifying Interfaces

- PEP -

## One Year Report

D.M. Stefanescu, PI, B.K. Dhindaw, CoPI, F.R. Juretzko, Gr. Res. Asst.  
*The University of Alabama*

P.A. Curreri, CoPI, S. Sen, CoPI  
*NASA - Marshall Space Flight Center*

S. Breeding, R. Spivey  
*TEC-Master*

During the LMS Mission on the space shuttle Columbia (between June 22 and July 6, 1996), three experiments were conducted to evaluate the effect of liquid metal convection on the phenomenon of particle engulfment and pushing by solidifying interfaces (*PEP*). This report includes the results obtained after one year of analysis of flight results. In addition, a succinct account of ground pre-flight results is included, so that an appropriate comparison can be made. Ground post-flight experiments were also performed, but their analysis is not complete at this time.

## 1. Objectives

During solidification of metal matrix composites the ceramic particles interact with the solidification front. This interaction is responsible for the final microstructure. The solutal and thermal field, as well as fluid motion at the liquid/solid interface influence both interface morphology and the particle/interface interaction itself. It is thus imperative to fully understand the solidification science and transport phenomena aspects associated with the process in order to control it.

The scientific objectives of this work include: 1) to enhance the fundamental understanding of the physics of interaction between inert particles and the solidification interface, and 2) to investigate aspects of melt processing of particulate metal matrix composites in the unique microgravity environment that will yield some vital information for terrestrial applications. The proposal itself calls for a long term effort on the Space Station. The LMS was a flight opportunity with limited scope. Its main objectives were as follows:

- to evaluate the experimental method including thermal regime, velocity regime, analysis procedures;
- to obtain preliminary data on the critical velocity of particle engulfment.

## 2. Background

The phenomenon of interaction of particles with melt interfaces has been studied since the mid 1960's. While the original interest in the subject was mostly theoretical, researchers soon came to the realization that understanding particle behavior at solidifying interfaces may yield practical benefits. The experimental evidence demonstrates that there exist a *critical velocity* of the planar solid/liquid (SL) interface below which particles are *pushed* ahead of the advancing interface, and above which particle *engulfment* occurs.

While the problem is relevant to many fields of work such as cryobiology, frost heave in soils, ceramic superconductors, etc., the majority of research work involving *PEP* is aimed at metal matrix composites. Here the driving force is to obtain a homogenous particle distribution. To achieve this goal one has to control the cooling conditions of cast composites in such a way that the

solidification velocity is higher than the critical velocity. Only with a homogeneous distribution of the reinforcement phase the improved mechanical properties of these materials can be fully exploited.

While numerous models have been proposed over the years in an attempt to explain particle behavior at the SL interface, a paucity of data exist in particular for ceramic particles dispersed in metal matrices. The basic assumptions of all models include spherical and inert particles, and macroscopically planar SL interface. Existing literature data on this subject are rather limited. With a few exceptions the SL interface, for which the data have been reported, is not planar. Thus, the results do not refer to the pushing / engulfment transition, but rather to pushing / entrapment. The particles used in most studies were not spherical but had an irregular shape, which runs against one of the basic model assumptions. These and other constrains of presently available experimental data make the task of model validation for metallic systems an impossible one. Accordingly, the main goal of the flight program is to provide reliable experimental data that can be used for validation of models describing particle behavior at the solidifying interface in metal matrix composite materials.

### 3. Methods of Data Acquisition and Analysis

#### 3.1 Selection of metal matrix - ceramic particle system

The metal matrix - ceramic particle system to be used for evaluation of the critical velocity for the pushing / engulfment transition (*PET*) must satisfy the requirements imposed by the major assumptions in existing particle pushing models. These assumptions include: pure metal matrix, planar SL interface, spherical particle, particle is chemically inert with respect to the metal, minimum liquid convection at the SL interface, no flotation or sedimentation of particles.

Based on these restrictions the experimental system chosen consisted of zirconia particles dispersed in a pure aluminum matrix. Aluminum (99.999% Al) was selected in spite of obvious difficulties resulting from its high affinity for oxygen, because it is the basis for the most promising cast metal matrix composites for mass production. In addition, an Al-4.5% Ni alloy was also prepared, to explore the implications of low solutal levels, and of change in wettability.

Zirconia particles were selected because they do not react with aluminum up to temperatures of 900 °C. While both zirconia and silicon carbide are non-wetting at 700 °C, as the temperature is raised to 1100 °C the SiC becomes wetting, indicating an interface reaction. Zirconia remains non-wetting. Additionally, ZrO<sub>2</sub> is thermodynamically more stable than Al<sub>2</sub>O<sub>3</sub>. Thus no reducing reaction is expected below 900 °C. Finally, spherical zirconia particles are available, while it was impossible to find spherical SiC particles.

The general shape of the zirconia particles is presented in Fig. 3-1. The nominal particle diameter was 500 μm. A size distribution of the particles is given in Fig. 3-2.



Fig. 3-1 SEM images of zirconia particles

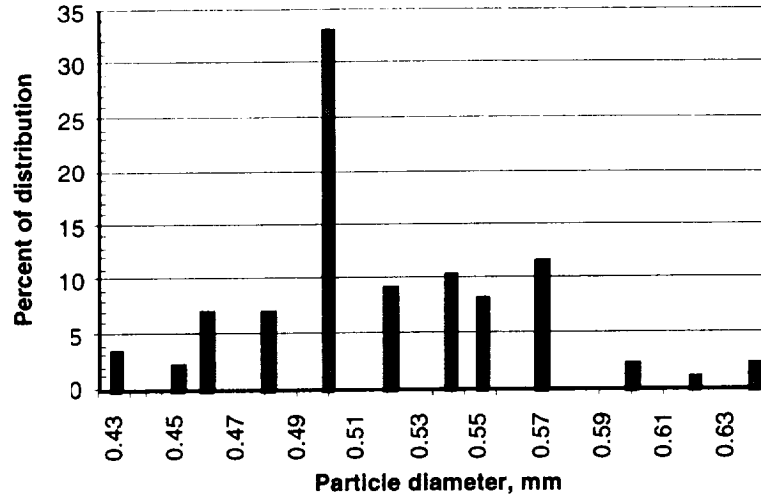


Fig. 3-2 Zirconia particle size distribution

### 3.2 Sample preparation

The same method was used for ground and flight sample preparation. The samples to be used for directional solidification were prepared by melt processing in a resistance furnace under high purity argon atmosphere and casting into a graphite mold to produce cylindrical specimens of 9 mm diameter and 100 mm length. Two to three vol.% zirconia particles were added to the liquid and mechanically mixed before pouring.

### 3.3 Evaluation of particle position

The zirconia particle distribution in the aluminum samples after casting and after DS was evaluated through real time X-ray Transmission Microscopy (*RXTM*). Magnifications of up to 20x were used. A three dimensional distribution of the particles was obtained by rotating the sample under the X-ray beam and recording the transmitted image on a video recording device.

In addition to *RXTM* all ground samples were examined by optical metallography. The samples were grounded layer by layer to map the volumetric particle location. About 200  $\mu\text{m}$  of material were removed each time. As the particles were 500  $\mu\text{m}$  in diameter it was possible to locate all of them. The flight samples will also be examined by optical metallography.

A number of criteria for interpretation of experimental results were established to obtain “clean” data for the evaluation of the *PET*, as follows:

- Particles were assumed to be *pushed* if:
  - for ground (quenched) samples: particles were found at or very near the quench interface;
  - for all samples: there were no particles in the middle of the sample in the DS region.
- Particles were assumed to be *engulfed* if:
  - for ground (quenched) samples: there were no particles at the quench interface.
  - for all samples: there were particles in the middle of the sample in the DS region;
- Clusters of particles were ignored.
- Particles at the following locations were ignored: the first 3 mm from the initial melt interface; the walls of the sample; particles attached to gas bubbles.

### 3.4 Ground pre-flight methodology

The ground samples (9 mm dia. x 100 mm length) were directional solidified in a Bridgman-type furnace. A total of 28 experiments were run with Al-ZrO<sub>2</sub> and 22 experiments were run with AlNi-

ZrO<sub>2</sub>. The gradients at the SL interface, as measured with the main heater temperature set at 800 °C and the trim heater temperature set at 850 °C, were 100 K/cm. For each sample only one translation velocity was used. After enough solid was produced through DS the crucibles containing the samples were quenched in water.

In DS experiments it is well known that the furnace translation velocity is not the same as the solidification velocity. To evaluate an *average solidification velocity*, the distance between the initial melt interface and the SL interface after quenching was measured and divided by the furnace translation time.

### 3.5 Flight methodology

During the LMS Mission three samples were directionally solidified in the AGHF facility. They will be referred here as flight samples FM1, FM2, and FM3. The main characteristics of the samples are summarized in **Table 1**. The ampoule-sample assembly for the three flight samples is shown in **Fig. 3-3**. Each ampoule-sample assembly was instrumented with 12 thermocouples. Three of these were placed into a ceramic sheath and incorporated into the sample by casting. The remaining eight were positioned in grooves on the outside of the crucible. Different furnace velocity regimes were used during the DS of the samples. For FM1 a step-wise decreasing regime was used, while for the other two a step-wise increasing regime was chosen. The exact numbers used for furnace translation velocity are given in **Table 1**. The flight data were recorded on a spreadsheet and included furnace position, furnace velocity, thermocouple position, and temperature for each thermocouple versus time. The SL interface velocity resulting from the different furnace translation velocities was calculated based on thermocouple data.

Table 1 Characteristics of flight samples

Flight sample	Material	Ampoule-sample	Velocity regime, $\mu\text{m/s}$
FM1	Al - ZrO <sub>2</sub>	spring-piston	20 - 5 - 0.5
FM2	AlNi - ZrO <sub>2</sub>	expansion reservoir	1 - 3 - 9
FM3	Al - ZrO <sub>2</sub>	expansion reservoir	1 - 3 - 9

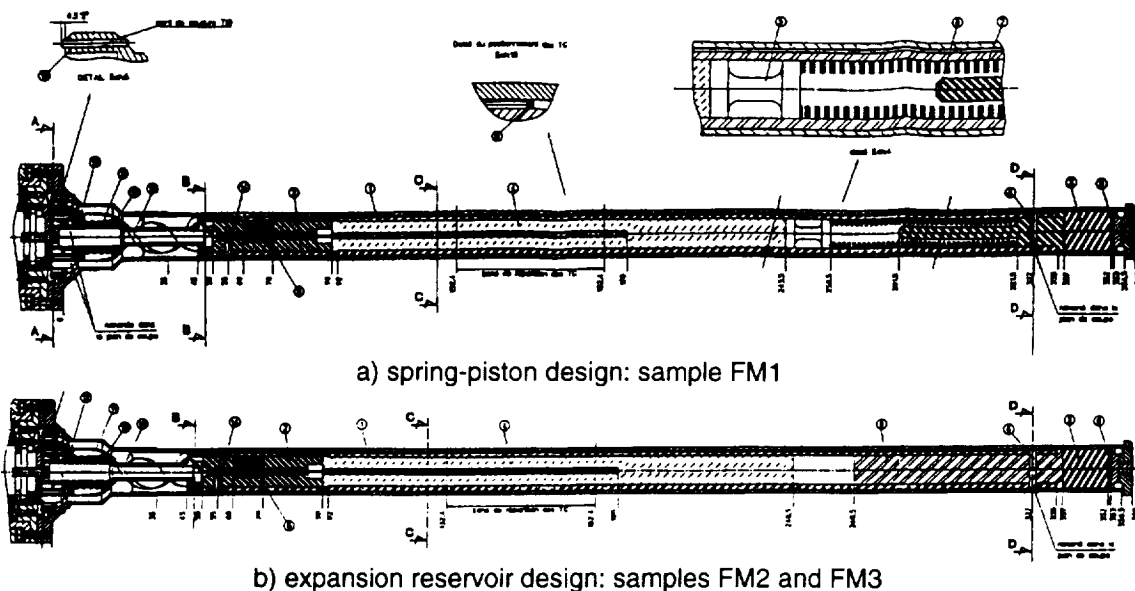


Fig. 3-3 Design of ampoule-sample assembly.

Each flight sample was examined after micro-g processing by X-ray computer tomography (CT) to assess its integrity.

## 4. Flight Results Compared with Ground Results

### 4.1 Ground results

From the 28 experiments run only 13 experiments were considered “clean” and were used for the evaluation of the *PET*. Some typical examples of particle distribution after DS are shown in Fig. 4-1. Note that on sample Al-14 two particles present in the DS region were not considered as engulfed because they were engulfed during the initial transient when the solidification velocity is not steady.

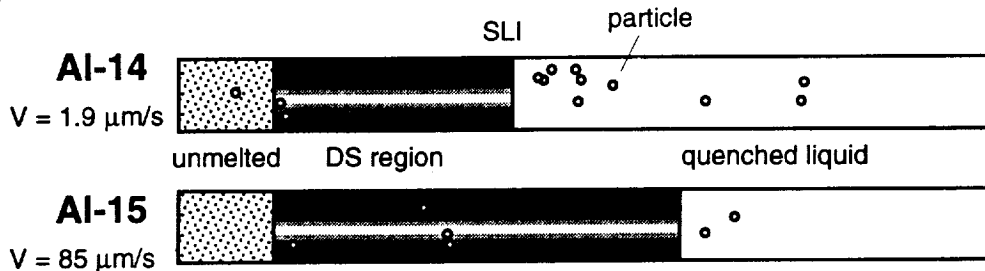


Fig. 4-1 Schematic representation of particle distribution in DS aluminum - zirconia samples: top - pushing; bottom - engulfment.

The results of the directional solidification experiments for the aluminum-zirconia system are summarized in Table 2. For ease of interpretation the data have been listed in increasing order of the solidification velocity at which they have been processed. From these data it is obvious that a clear *PET* exists at a solidification velocity between 1.9 and 2.4  $\mu\text{m/s}$ . However, a notable exception is seen for sample Al-18.

Table 2 Experimental results for aluminum - zirconia samples

Solidification velocity, $\mu\text{m/s}$	1.3	1.3	1.5	1.9	2.4	2.6	5.8	6.5	10.9	10.9	15	44.8	85
Sample no.	Al-22	Al-27	Al-28	Al-14	Al-23	Al-21	Al-29	Al-30	Al-17	Al-18	Al-24	Al-16	Al-15
Result*	P	P	P	P	E	E	E	E	E	P	E	E	E

\* P: pushing, E: engulfment

For the AlNi-zirconia system particles were engulfed at all velocities used, that is from 1.2 to 80  $\mu\text{m/s}$ . Thus, it is apparent that the *PET* should occur at velocities smaller than 1.2  $\mu\text{m/s}$ . This lower range of velocities is beyond the present capabilities of the UA furnace.

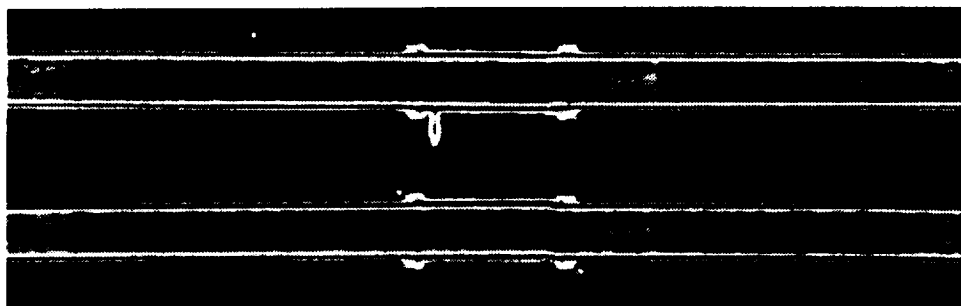
### 4.2 Flight results

#### 4.2.1 Engineering report

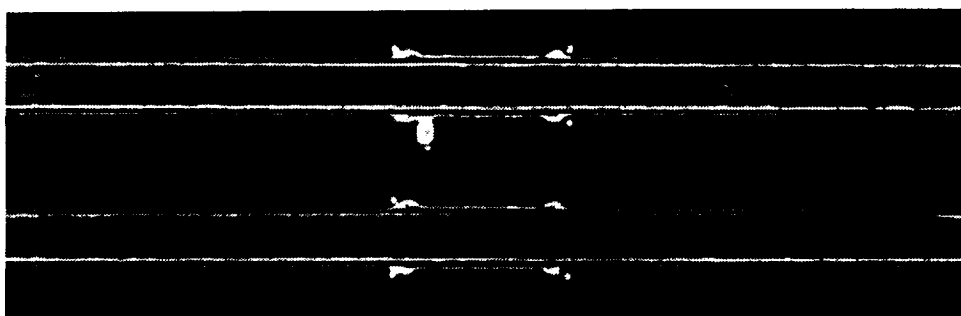
Both the cartridge containing the ampoule, and the ampoule after extraction from the cartridge were examined by X-ray and computer tomography (CT). The results of the cartridge CT evaluation are shown in Fig. 4-2.

The spring-piston assembly used for sample FM1 functioned as expected. Some liquid Al leak is seen past the fore side of the piston. This leak does not seem to be significant, since no Al is seen in the 90° position of the CT (lower picture on Fig. 4-2a). No metal has leaked past the aft side of

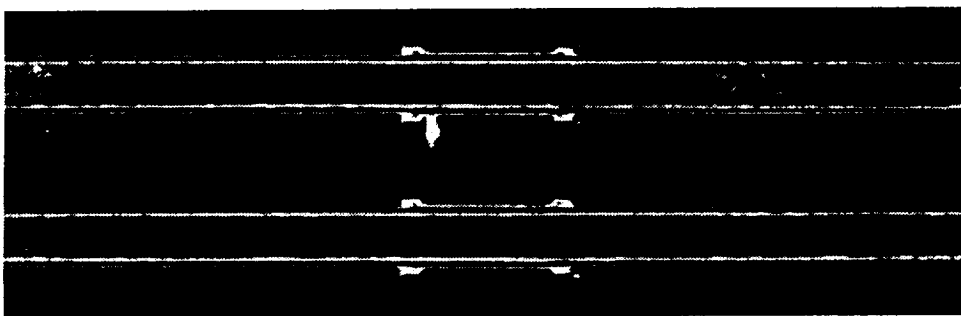
the piston, and the nominal operation of the spring-piston assembly was not affected. As a result of this no void is seen between the piston and the sample and the sample itself was sound.



a) sample FM1



b) sample FM2



c) sample FM3

Fig. 4-2 CT images of the flight cartridge - ampoule assembly.

Sample FM2 was less successful. On **Fig. 4-2b** it is seen that several voids have formed along the sample. It appears that the liquid metal has fractured in that region resulting in a two-part solid sample: an upper part that is in contact with the alumina plug, and a lower part.

Sample FM3 behaved as expected. On **Fig. 4-2c** it is seen that the shrinkage cavity was positioned between the metal and the alumina plug. The sample itself appears to have no significant shrinkage porosity or voids.

#### 4.2.2 Science report

Samples FM1 and FM3 which consisted of Al-ZrO<sub>2</sub> will be discussed first. A summary of *RXTM* particles positions in the FM1 sample before and after flight is given in **Fig. 4-3**. To identify the particles positions with respect to velocity zones, a velocity-distance graph was associated with the *RXTM* images. It is quite clear that at velocities of 5  $\mu\text{m/s}$  and above all particles were engulfed. A more detailed analysis is necessary for the region solidified at 0.5  $\mu\text{m/s}$ . To this effect the region of

interest was enlarged in Fig. 4-4. It is seen that as the SL interface velocity decreases from 5 to 0.5  $\mu\text{m/s}$  particles are still engulfed ( no.1, 2 and 3). In the region of 0.5  $\mu\text{m/s}$  all particles have been pushed by the interface, with the exception of particle no. 4. However, upon rotating the sample during *RXTM* examination it was found that this particle is very close to the crucible wall, which means it should be removed from consideration. As soon as the velocity increases due to rapid furnace translation at the end of the experiment particles are engulfed (no. 5). A detailed *RXTM* image of the region of interest is presented in Fig. 4-5.

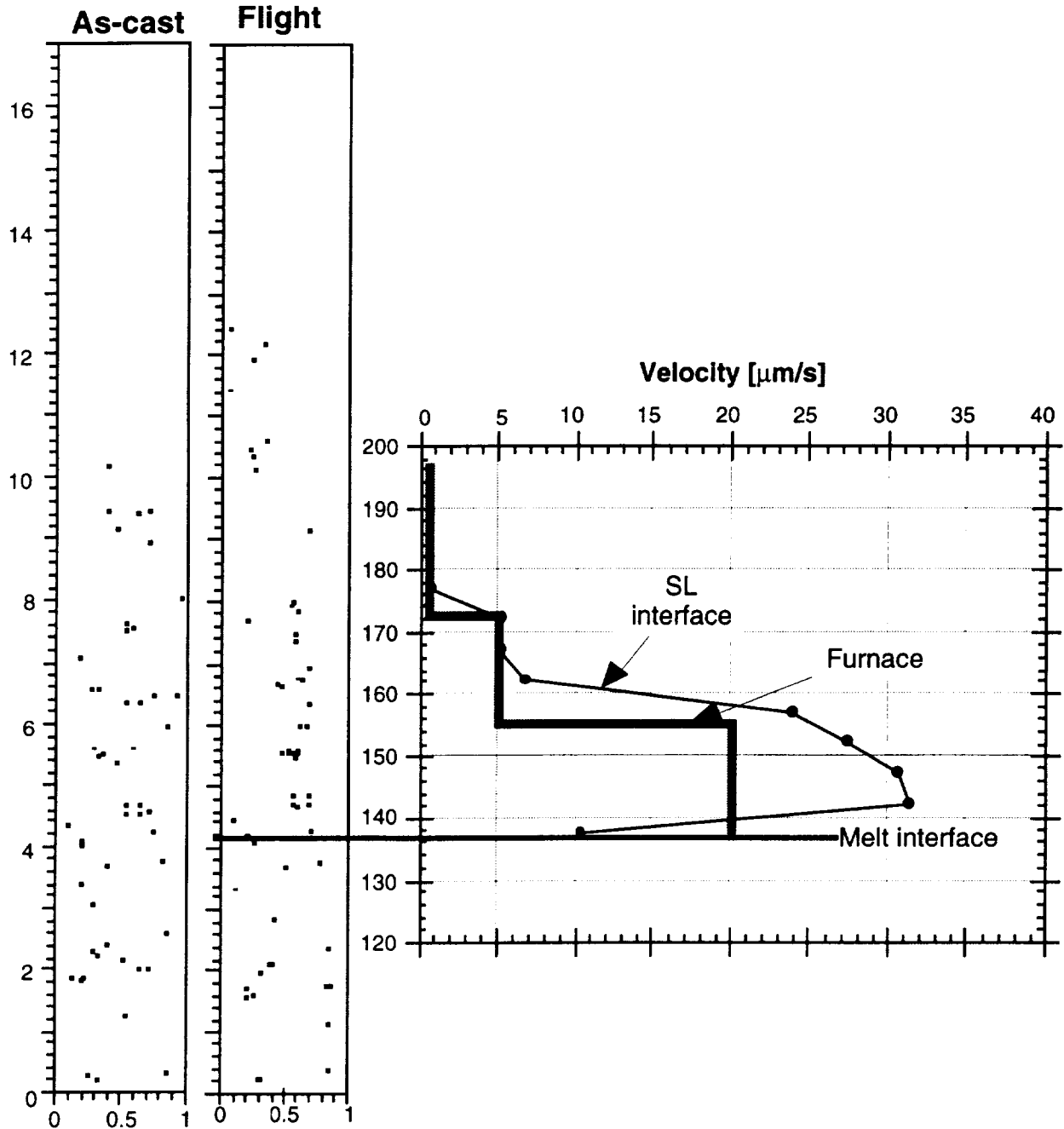


Fig. 4-3 Summary of *RXTM* evaluation of particles positions correlated to furnace and solid/liquid interface velocity for sample FM1.

It must be noted that the interface velocity could be accurately determined only as long as thermocouple information was available. Then, since in the 0.5  $\mu\text{m/s}$  regime our calculations indicated that furnace velocity and interface velocity were linear and had approximately the same slope, the position of the SL interface was extrapolated as shown in Fig. 4-4.

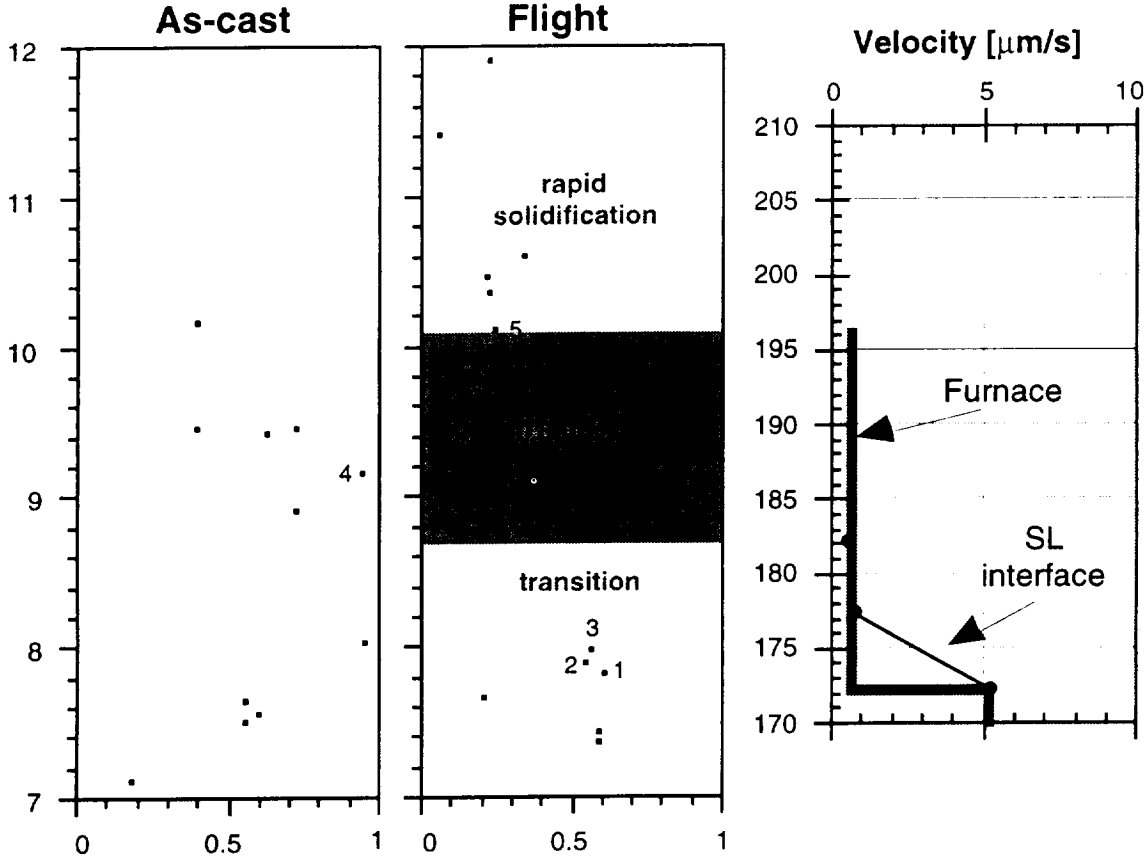


Fig. 4-4 Summary of *RXTM* evaluation of particles positions in sample FM1 in the region of furnace translation rate of 0.5  $\mu\text{m/s}$ .

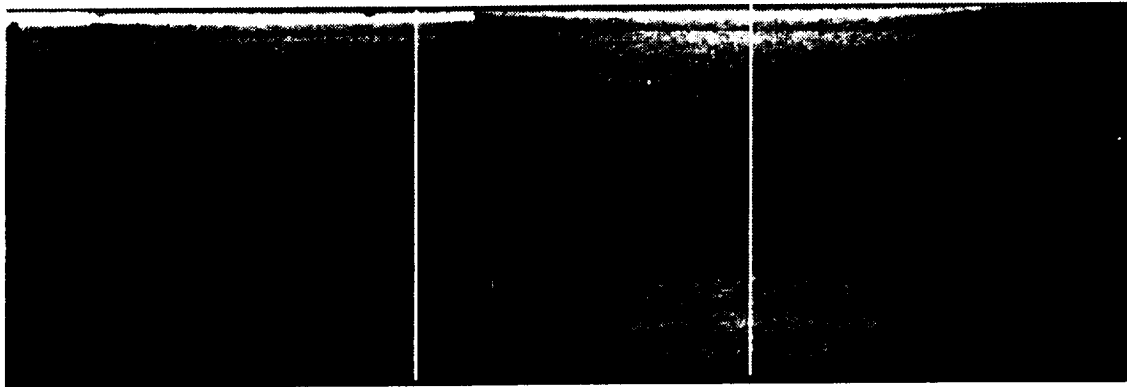


Fig. 4-5 *RXTM* image of flight sample FM1. Particles are engulfed at 5  $\mu\text{m/s}$  and in the transient region. No valid engulfed particles are present in the 0.5  $\mu\text{m/s}$  region.

From the analysis of *RXTM* particles position in the FM3 sample before and after flight (Fig. 4-6) it is concluded that, since particles are found in all three velocity regions, engulfment occurred even at the lowest velocity regime used in this sample, which was of 1  $\mu\text{m/s}$ .

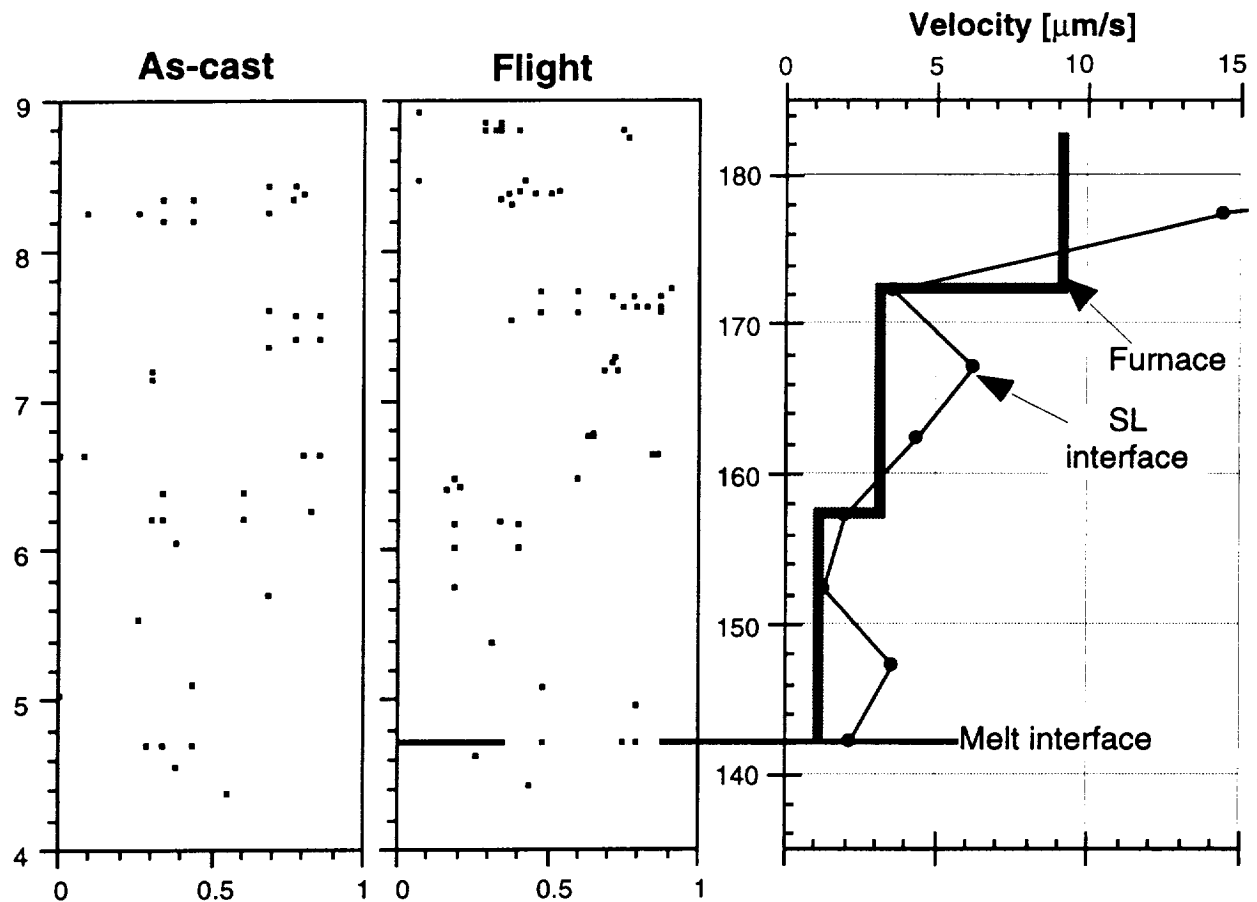


Fig. 4-6 Summary of *RXTM* evaluation of particles positions in sample FM3 in the region of furnace translation rate of 1 and 3  $\mu\text{m/s}$ .

The material used for sample FM2 was  $\text{AlNi-ZrO}_2$ . The *RXTM* particles position in this sample is presented in Fig. 4-7. From the analysis of these data it is apparent that the target interface velocity of 1  $\mu\text{m/s}$  has been achieved only on a very narrow region of the sample. It is not clear if pushing occurred in that region. It was also observed, even by *RXTM*, that many particles have reacted, in particular toward the end of the sample. Clearly, metallographic analysis and additional experiments are required to allow for any definitive conclusions.

### 4.3 Discussion

One of the basic criteria for acceptability of *PEP* experimental results is an *inert particle / matrix* system. Thus, before any definitive conclusions could be reached on any of the flight samples, it must be documented that no reaction occurred at the particle / matrix interface. At this time only some preliminary results are available on sample FM3. They are illustrated in Fig. 4-8. It is seen that as long as moderate temperatures were reached during processing a clean particle / matrix interface is obtained. The white borders on Fig. 4-8a are only shadows. However, at temperatures higher than 900  $^{\circ}\text{C}$ , EDAX analysis confirmed that zirconia particles reacted with the matrix, producing an oxidized interface (Fig. 4-8b). The oxidized region is  $\text{Al}_2\text{O}_3$ . It is thus clear that a complete analysis of particle /matrix interface must be conducted for the regions of interest.

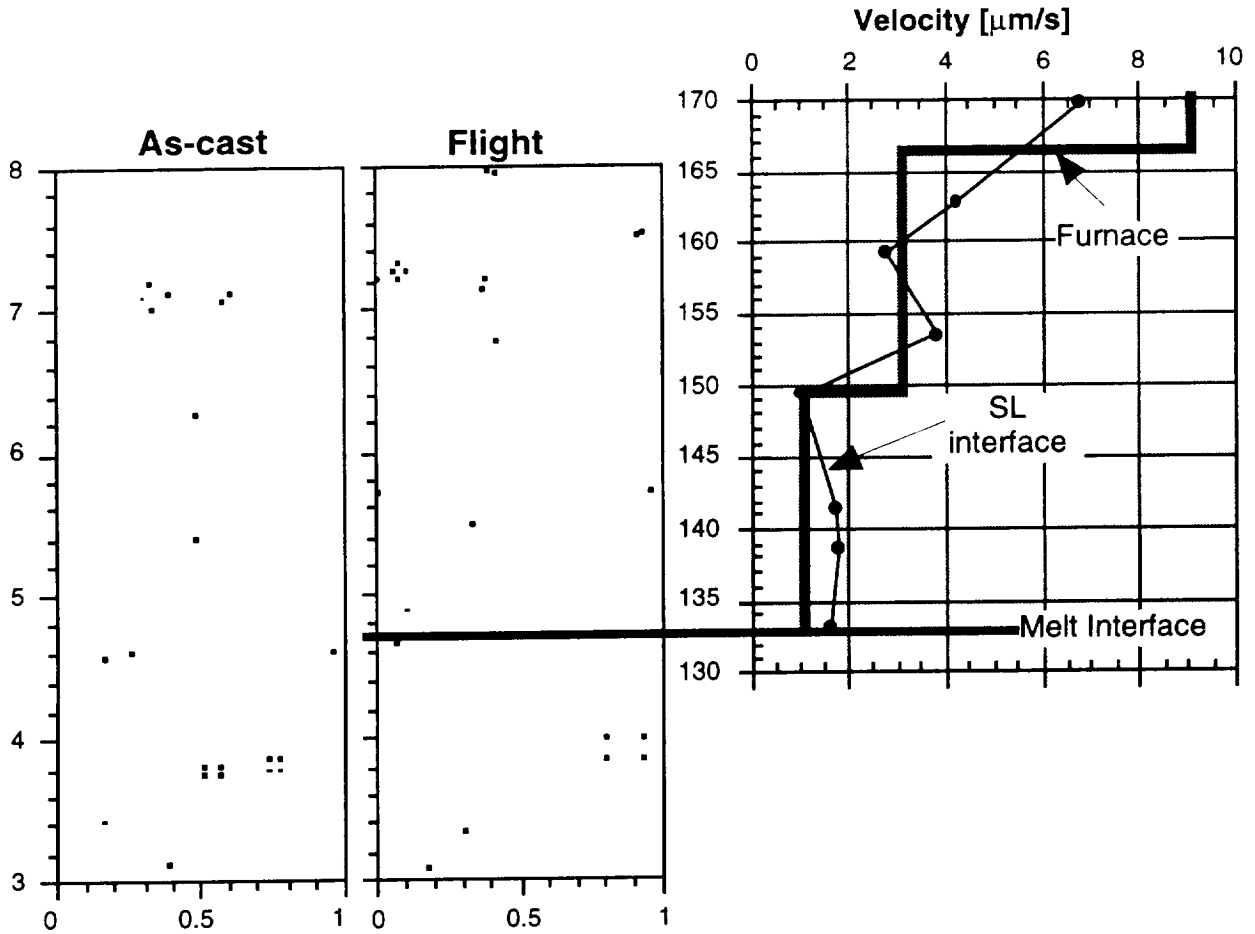
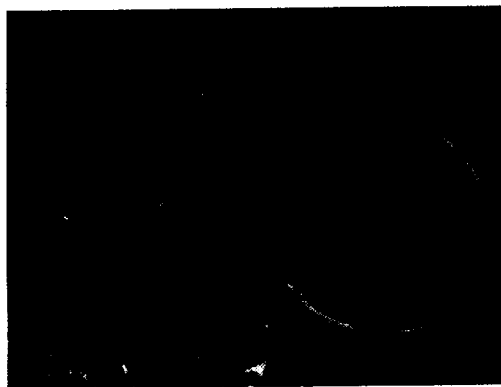
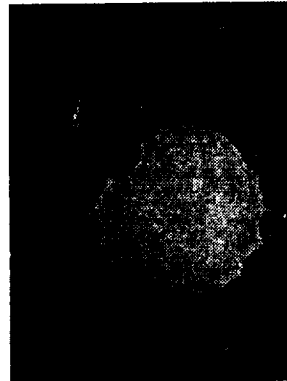


Fig. 4-7 Summary of *RXTM* evaluation of particles positions in sample FM2 in the region of furnace translation rate of 1 and 3  $\mu\text{m/s}$ .

Assuming for the time being that in the controlled DS regions of the samples zirconia particles did not react, it seems to be possible to conclude that the absence of convection resulted in a decreased critical velocity. Indeed, for the Al-ZrO<sub>2</sub> system flight results seem to indicate a critical velocity between 0.5 and 1  $\mu\text{m/s}$ , while ground experiments suggest a critical velocity between 1.9 and 2.4  $\mu\text{m/s}$ .



a) good interface in the DS region at 710 °C



b) oxidized interface in DS region at 950 °C

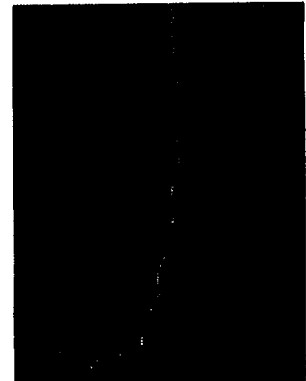


Fig. 4-8 SEM evaluation of particle (zirconia) - matrix (Al) interface

These results are not surprising. Indeed, work with organic transparent materials has also demonstrated that the critical velocity increases with the level of convection in the liquid, and that above a certain convection level the particle does not interact with the interface at all<sup>1</sup>.

Fluid mechanics also provides arguments for this behavior. Assuming that the particle moves parallel to the SL interface because of natural convection (Fig. 4-9), it can be expected to roll because of the velocity gradient imposed in the y-direction. Simple calculations for ideal fluids show that in such a case a "lift" force will be generated<sup>2</sup>. This force will act in the y-direction and will be directed away from the interface. This force is accentuated when the particle moves at a velocity different from the average fluid flow rate<sup>3</sup>. The lift force will thus behave like an additional repulsive force and therefore will increase the critical velocity.

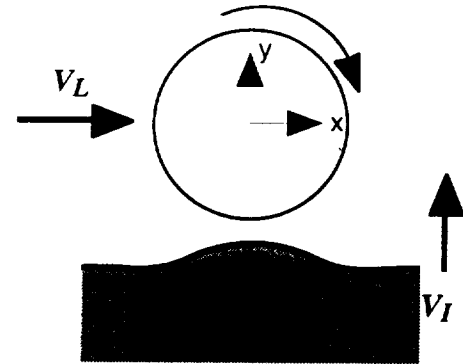


Fig. 4-9 Origin of the lift force.

## 5. Conclusions

The main conclusions that can be drawn at this time are as follows:

- A flight methodology has been developed and successfully tested.
- Pushing has been observed in the Al-ZrO<sub>2</sub> system at a solidification velocity of 0.5 μm/s. Engulfment was observed at velocities of 1 μm/s and above. This seems to indicate a critical velocity for PET of 0.5 to 1 μm/s.
- In the AlNi-ZrO<sub>2</sub> system pushing may have been observed at 1 μm/s. However, no firm conclusion could be reached at this time.
- The present results may only be considered as preliminary. A significantly larger number of samples must be processed in order to confirm the present conclusions.

## 6. Bibliographic Citations

- H. T. Pang, D. M. Stefanescu and B. K. Dhindaw, "Influence of Interface Morphology on the Pushing/Engulfment Transition of Polystyrene Particles in Succinonitrile + Water Matrices," in *Cast Metal Matrix Composites*, Proceedings of the 2nd International Conference, D. M. Stefanescu and S. Sen editors, AFS, Des Plaines, Illinois (1994) 57-69
- H. Pang and D. M. Stefanescu, "Influence of Interface Morphology on the Pushing/Engulfment Transition of Polystyrene Particles in Succinonitrile + Water Systems," in *Experimental Methods for Microgravity Materials Science Research*, R. A. Schiffman and B. Andrews editors, TMS Warrendale, Pa (1994), 209-213
- D. M. Stefanescu, R. V. Phalnikar, H. Pang, S. Ahuja and B. K. Dhindaw, "A Coupled Force Field-Thermal Field Analytical Model for the Evaluation of the Critical Velocity for Particle Engulfment", *ISIJ International* 35, 6 (1995) 700-707
- F.R. Juretzko, D.M. Stefanescu, B.K. Dhindaw and S. Sen, " Interfacial Energy  $\Delta\gamma$  - Theoretical and Experimental Evaluation For Metal-Ceramic Systems," in *Processing, Properties and Applications of Cast Metal Matrix Composites*, P.K. Rohatgi editor, The Minerals, Metals & Materials Society (1996) 21-31
- S. Sen, B.K. Dhindaw, D.M. Stefanescu, A. Catalina and P.A. Currei, "Melt Convection Effects on the Critical Velocity of Particle Engulfment", *J. Crystal Growth* 173, 3-4 (1997) 574-584

## 7. Non-technical Summary

In this experiment zirconium oxide particles dispersed in liquid aluminum were used to model what happens to inert, nonreactive particles at the solid-liquid interface in different systems. Convection, and thus movement in the liquid, complicates the physics of the material interaction on Earth. By conducting this investigation in microgravity these difficulties could be overcome. When discrete particles are present in a liquid matrix, directional solidification of the liquid will either cause the particles to become engulfed in or pushed out of the solid. Whether particles are engulfed or pushed depends on the speed of solidification. If the solidification velocity is higher than a certain critical velocity, the particles are engulfed by the advancing solid; if it is lower, they are pushed ahead of the solid.

Modeling these systems has future applications in fields ranging from superconductor and metal matrix composites to frost heaving and cryobiology. For example, particle engulfment is beneficial when creating metal matrix composites, which are metals that incorporate strengthening particles, usually of a ceramic material, for reinforcement. Engulfment of these particles results in their being uniformly distributed, giving the composite material better properties than if the particles were pushed during solidification. In addition, understanding the physics behind particle engulfment and pushing can lead to solutions to problems like frost heaving. Frost heaving occurs when water that has seeped around soil begins to freeze. Because the solidification velocity of the water is slower than the critical velocity for engulfment, the soil particles are pushed out of the solid water (ice), causing the combination of ice and soil to take up as much as 300 percent of the volume of the original soil and water mixture. The increase in volume can displace road surfaces and foundations, causing a great deal of damage. The exploration of these physical phenomena may provide a stepping stone for those who wish to conquer such earthly problems.

## References

- 
- <sup>1</sup> S. Sen, B.K. Dhindaw, D.M. Stefanescu, A. Catalina and P.A. Curreli, *J. Crystal Growth*, **173**, 3-4 (1997) 574-584
  - <sup>2</sup> R.H. Nunn, *Intermediate Fluid Mechanics*, Hemisphere Publishing Co., New York (1989) 51-55
  - <sup>3</sup> P.G. Saffman, *J. Fluid Mechanics*, **31** (1968) 624

